Water and ion transport in human skin after application of saline solution

Houben, M.M.J.

Award date:
1997

Master of Science Thesis
Eindhoven University of Technology
Department of Mechanical Engineering
Division of Computational and Experimental Mechanics

Water and ion transport in human skin after application of saline solution

M.M.J. Houben

WFW report 97.079
December 1997

Research carried out from January 1997 to December 1997 at
Personal Care Institute, Philips Research Laboratories Eindhoven
Commissioned by prof. dr. ir. J.D. Janssen (TUE)
Under supervision of dr. ir. L.F.A. Douven (Philips), dr. ir. J.M.R.J. Huyghe (TUE) and ir. P.M. van Kemenade (TUE)

Abstract

Due to the higher water content in the human body as compared to the dry environment, water is continuously lost through the skin. The amount of water leaving the body through the skin to the environment in the absence of sweating, is called the transepidermal water loss (TEWL).

TEWL is measured by the Evaporimeter, based on the measurement of the water vapour pressure gradient immediately adjacent to the surface of the skin. The physical properties of skin are influenced by the water content or hydration. The Corneometer quantifies the hydration state of skin by measuring the electrical capacitance. In experiments, TEWL and electrical capacitance (measure of hydration state) are measured on the volar forearm of volunteers, after application and removal of saline solution. The results show that TEWL increases after application of water or a salt solution of either 1 M or 4 M. The higher TEWL exponentially decreases in time until pre-application values are obtained. With increasing molarity TEWL reaches these values more rapidly. The electrical capacitance shows a large variation over the subjects and does not retrieve pre-application value. It is uncertain whether the measured capacitance is a correct measure of hydration under these experimental circumstances.

Water and ion flow in skin is simulated by using a quadriphasic mixture model for skin coupled with a diffusion model for water vapour transport in air. Simulation of hydration (exposure of skin to a salt solution) seems to reflect the expected physiological responses. A linear concentration profile develops and the skin swells. When the hydrated skin is exposed to air, the displacements and concentrations respond as expected. The skin shrinks and the concentrations rapidly decrease. However, the fluid flow is higher than observed in the experiments and remains almost constant in time. This may be due to a limited water inflow at the bottom side, or a shift of the main barrier against waterloss from the very surface to deeper in the skin.

"Beauty is but skin-deep."

Contents

List of symbols

Symbols

a^β	activity of component β, defined as $a^\beta = f^\beta c^\beta$
$\mathcal{A}$	surface
c^β	concentration per unit fluid volume of component β
c^{fc}	concentration per unit fluid volume of the fixed charges in equivalent moles of univalent ions per unit volume
$\overline{c}$	concentration of external salt per unit fluid volume
$\boldsymbol{D}^\alpha$	diffusion tensor of ion α
$\boldsymbol{D}^v, D^v$	diffusion tensor/scalar of water vapour in air
$\boldsymbol{E}$	Green-Lagrange strain tensor
E	Young's modulus
f^β	activity coefficient of component β
F	Faraday's constant
$\boldsymbol{F}$	deformation tensor
h	weighting function
J	$= \det(\boldsymbol{F}) = dV/dV_0$, relative volume change
$\boldsymbol{K}$	permeability tensor
M	molar mass
n^α	volume fraction of component α
$\vec{n}$	outward unit normal on surface
p	fluid pressure
p^v	partial vapour pressure
rh	relative humidity
R	universal gas constant
t	time
T	absolute temperature
$\vec{v}^\alpha$	velocity vector of component α
$\vec{v}^{\beta s}$	$= \boldsymbol{F}^{-1} \cdot (\vec{v}^\beta - \vec{v}^s)$
$\overline{V}^\beta$	partial molar volume of component β
$\mathcal{V}$	volume
W	Helmholtz free energy of the mixture
ζ	shape function
θ	time integration constant
μ^β	electro-chemical potential of component β

ν	Poisson's ratio
ξ	electrical potential per unit volume constituent
π	osmotic pressure
ρ	density
$\boldsymbol{\sigma}$	Cauchy stress tensor
$\boldsymbol{\sigma}^{\mathit{eff}}$	effective stress tensor, defined as $\boldsymbol{\sigma}^{\mathit{eff}} = \boldsymbol{\sigma} + p\boldsymbol{I}$
ϕ^{β}	osmotic coefficient of component β
ψ	matric potential

Subscripts

0	reference state
env	environment
sat	saturated

Superscripts

eff	effective
f	fluid
fc	fixed charge
s	solid
v	vapour
$+$	cations (positive ions)
$-$	anions (negative ions)
α	arbitrary component (s, f, $+$ or $-$), unless stated otherwise
β	any of the components fluid or ions (f, $+$ or $-$)

Notation

a, A	scalar
$\vec{a}$	vector
$\boldsymbol{A}, \boldsymbol{\sigma}$	second order tensor
$\overline{a}$	the bar denotes values in the outer solution (except for $\overline{V}^{\beta}$ in which the bar indicates a partial molar quantity)
$\underset{\sim}{a}$	column representation
$\underline{\underline{A}}$	matrix representation
$\boldsymbol{A}^{c}$	conjugate of $\boldsymbol{A}$
$\boldsymbol{A}^{-1}$	inverse of $\boldsymbol{A}$
$\mathrm{tr}(\boldsymbol{A})$	trace of $\boldsymbol{A} = \boldsymbol{A} : \boldsymbol{I}$

$\cdot$	dot vector (tensor) product operator
$\vec{\nabla}$	Eulerian gradient operator
$\vec{\nabla}_0$	$= \boldsymbol{F}^c \cdot \vec{\nabla}$, Lagrangian gradient operator
$\frac{\partial a}{\partial t}, \dot{a}$	partial time derivative of scalar a
$\frac{\mathrm{D}^\alpha a}{\mathrm{D}t}$	$= \frac{\partial a}{\partial t} + \vec{v}^\alpha \cdot \vec{\nabla} a$, component α material time derivative (Lagrange) of scalar a

Chapter 1

Introduction

Due to the higher water content in the human body as compared to the environment, water is continuously lost through the skin to the environment. The present report describes the research on transport phenomena in skin. This research is the final project for the Biomechanical Engineering curriculum at the Eindhoven University of Technology. The project was performed at the Personal Care Institute, situated at the Philips Research Laboratories in Eindhoven.

The aim of this project is to measure and simulate the water and ion transport through the skin, under varying (environmental) conditions. The ultimate goal is a better understanding of the skin's condition and healing mechanisms in undamaged and damaged skin.

The amount of water leaving the body through the skin to the environment in the absence of sweating is called transepidermal water loss (TEWL). This water loss depends on the difference in vapour pressure between the skin surface and the environmental vapour pressure. In experiments, transepidermal water loss and electrical capacitance are measured on the forearm of volunteers after application and removal of a saline solution of varying molarity.

Mixture models are used to describe transport phenomena in skin. Van Kemenade uses a triphasic mixture model for skin involving: (1) a solid, (2) a fluid, and (3) an ionic component [Van Kemenade *et al.* '97]. Laws of balance deduced for each component are combined with interaction terms (mixture approach). All ions (positive and negative) are treated as one component, neglecting electrical effects. However, these electrical effects may not be negligible due to the presence of negatively charged macro-molecules (fixed charge density) in skin. The charged macro-molecules are suspected to exert a high adsorption force upon the water (Donnan osmosis).

Frijns programmed a one dimensional quadriphasic mixture model distinguishing: (1) a charged solid, (2) a fluid, (3) a cationic, and (4) an anionic component [Frijns '96]. The quadriphasic mixture model includes electrical fluxes and potential gradients and can be transformed into the triphasic mixture model by setting the fixed charge density to zero. As it is programmed in the package Matlab, it offers a far more flexible tool than the triphasic skin model which is programmed in the complex finite element package DIANA. Switching the boundary condition of skin from a fluid boundary to an air boundary is far more easy to achieve in Matlab than in DIANA. The quadriphasic theory is able to describe deformation of the solid caused by mechanical (pressure), chemical (external concentration), or electrical load.

The purpose of this study is (1) to extend the finite element formulation of the quadriphasic

mixture model of skin with a diffusional water evaporation model of air, (2) to measure transepidermal water loss and electrical capacitance values after application of saline solution, and (3) to compare experimental and numerical results.

The subject of chapter 2 of this report is human skin and its water loss. Chapter 3 describes the methodology of the experiments and presents the resulting experimental data. Chapter 4 deals with the quadriphasic mixture model of skin, the diffusion model of water evaporation in air, and the numerical results. In chapter 5 the conclusions are summarised and recommendations are made.

Chapter 2

Human skin

In this chapter a brief description of the anatomic structure and function of human skin is given and the methods to measure water loss and skin hydration, used in the experiments, are described.

2.1 Structure and function of human skin

The skin is the largest organ of the human body, with a total surface between 1 and 2 m^2 and a mass between 4 and 7 kg. It has a stratified structure and three main layers are distinguished [Guyton & Hall '96]: the epidermis, the dermis and the hypodermis (see figure 2.1).

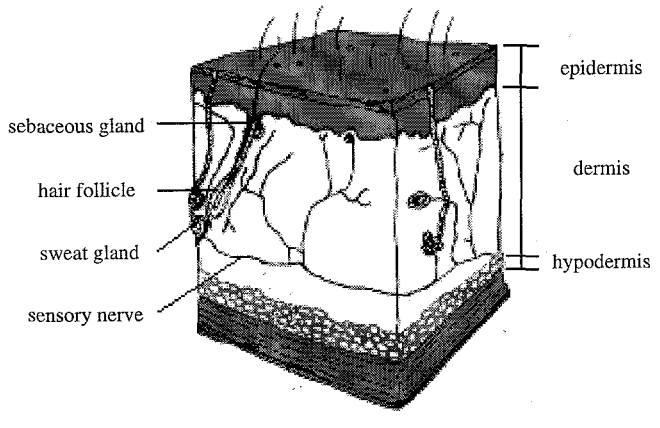

Figure 2.1: A schematic representation of human skin.

The epidermis; This upper epithelial layer is subdivided into four or five layers, distinguishing themselves by the state of differentiation and keratinisation of their most numerous cells, the keratinocytes. The stratum corneum, also known as the "horny layer", is the topmost layer, consisting of flattened, keratinised cells which are horny, hard, metabolically inactive, and do not contain a nucleus. These outer cells are constantly being shed and replaced from the layers below. The stratum corneum's barrier function prevents

excessive evaporation of body fluids and penetration of chemical substances. Melanin produced by pigment cells or melanocytes, attributes to the pigmentation of skin.

The dermis or cutis; This layer of connective tissue, situated immediately below the epidermis, contains blood vessels, lymph vessels, and nerves and is the largest layer of the skin. The dermis is composed of fibres in an amorphous ground substance. Three different fibres are (1) collagen which gives the skin its toughness and resilience, (2) elastin which gives the skin its elasticity, and (3) reticulin which is thought to be immature collagen. The ground substance consists of water molecularly bound to glycosaminoglycans (GAG's), proteins, enzymes, metabolites and other substances. Structures found within the dermis are sebaceous glands, sweat glands, arrector pili muscles, and hair follicles. Sebaceous glands secrete sebum via the hair follicles on to the stratum corneum. Sebum lubricates the skin and hair and is responsible for the formation of an 'acid mantle' (a fine film of sebum and sweat) and a waterproof hydro-lipid film on the skin's surface.

The hypodermis or subcutis; This is a fatty layer of loose connective tissue, which establishes a movable connection with underlying structures.

The skin plays an important physiological role in daily life. It protects the human body by means of a structured, adaptable barrier between the internal milieu and the external environment. Three main skin functions can be distinguished:

- **Protection** against
  - ☐ dehydration (primarily accomplished by the stratum corneum),
  - ☐ mechanical impacts like knocks and blows (epidermis and dermis),
  - ☐ ultraviolet rays (melanocytes),
  - ☐ micro organisms and chemical substances (acid mantle and stratum corneum),
  - ☐ external or internal aggressors on cellular level (polynucleines and macrofages).
- **Heat regulation** by
  - ☐ perspiration (eccrine sweat-glands),
  - ☐ insulation (fat cells),
  - ☐ heat transfer (vaso-dilatation and vaso-constriction).
- **Sensation** (due to the abundant supply of sensory nerves) of

  heat, cold, pain, itch, touch, and pressure.

2.2 Transepidermal water loss & hydration

Due to the higher water content in the human body as compared to the dry environment, water is continuously lost through the skin. The amount of water leaving the body through the skin to the environment in the absence of sweating, is called the transepidermal water loss (TEWL). It is influenced by the environment (air temperature, relative humidity) and the condition of the skin (individual variation, occlusion, damage of the stratum corneum, etc.).

The measurement of TEWL [kg·m^{-2}·s^{-1}] is based on the measurement of the water vapour pressure gradient immediately adjacent to the surface of the skin [Nilsson '77]:

$$\text{TEWL} = D' \frac{\partial p}{\partial x}, \tag{2.1}$$

with D' the diffusion coefficient for water-vapour in air [kg·m^{-1}·s^{-1}·Pa^{-1}], dependent on the temperature and atmospheric pressure, but approximated by a constant, and $\frac{\partial p}{\partial x}$ the vapour pressure gradient [Pa·m^{-1}]. [Nilsson '77] has shown that close to the surface the vapour pressure gradient is approximately constant. It is obtained by calculating the vapour pressure at two points near the surface of the skin using the formula:

$$p = \frac{rh}{100} \cdot p_{sat}, \tag{2.2}$$

where rh is the relative humidity [%] and p_{sat} the saturated vapour pressure [Pa], which is a function of the temperature alone. The measurement is accomplished by a cylindrical chamber with two humidity and temperature sensors at two separate fixed points situated on a line perpendicular to the surface and in the zone of diffusion (see figure 2.2).

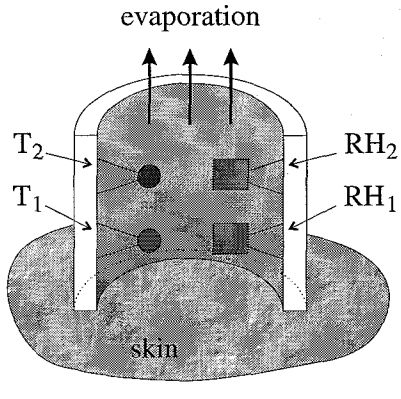

Figure 2.2: Illustration of a TEWL measurement device and its arrangement of sensors (adapted from [Nilsson '77]). T_1, T_2 and RH_1, RH_2 are pairs of thermometers and hygrometers, respectively.

Two commercially available TEWL instruments based on this principle are the Evaporimeter® developed by ServoMed (Stockholm, Sweden) and the Tewameter® developed by Courage-Khazaka (Cologne, Germany). Both instruments are adequate non-invasive TEWL instruments [Barel & Clarys '95]. The measurements in this report have been performed with the Tewameter. The probe is cylindrical with a diameter of 10 mm, height 20 mm and the sensors positioned at 2 and 4 mm distance from the skin surface.

Environmental factors such as external temperature, relative humidity and temperature of the probe influence the TEWL values and should therefore be controlled [Pinnagoda *et al.* '90]. Age (in the adult), sex, and race have no apparent effect on TEWL, whereas anatomical site, physical, thermal or emotional sweating and skin surface temperature (mainly the result of the ambient air temperature) influence TEWL [Hattingh '72, Pinnagoda *et al.* '90]. Preconditioning of the test person by 30 minutes of rest and measuring under standardised conditions – especially ambient air temperature and relative humidity controlled – is recommended.

Because the physical properties of skin (especially the stratum corneum) are influenced by the water content, reliable quantification of water content in the skin is of importance for understanding skin physiology. An instrument to quantify the hydration state of skin is the Corneometer® CM 820 developed by Courage-Khazaka (Cologne, Germany). This instrument measures the electrical skin capacitance by applying alternate voltage with a frequency of 40–75 kHz [Berardesca '97, Zuang *et al.* '97]. The manufacturer claims that this quantity is a measure of epidermal hydration down to a depth of 30 μm while [Blichmann & Serup '88] have reported a depth of about 60–100 μm. The instrument expresses the capacitance values in arbitrary units (a.u.). The probe (surface area 0.95 cm^2) consists of an interdigital grid of gold-covered electrodes functioning as capacitor plates and covered with a plastic foil 20 μm thick. No current passes through the skin, but an electric field is formed in the stratum corneum and the underlying layer of the epidermis. The electrode together with the upper part of the epidermis works as a variable capacitor. The capacitance value is influenced by changes in the dielectric constant of the skin which depends (in a non-linear way) on the skin's hydration [Tagami *et al.* '80, Zuang *et al.* '97].

The specific conditions under which the measurement is a correct measure of hydration level is not specified by the manufacturer. As in our application we use the instrument in unusual conditions – we expose the skin to salt solutions of varying concentrations – we are cautious about interpreting the measured values as hydration. In this report, the measured values given by the Corneometer will be referred to as capacitance. Other electro-measurement principles, found in literature, that have been used for the study of skin moisture content are impedance, e.g. [Ollmar & Emtestam '92, Tagami '88, Thiele & Malten '73] and its reciprocal, conductance, e.g. [Barel & Clarys '97, Berardesca '97, Blichmann & Serup '88, Graves *et al.* '95, Stender *et al.* '90, Tagami *et al.* '80, Tagami *et al.* '82, Tagami '82].

Chapter 3

In vivo measurements on human skin after application of saline solution

Experiments on volunteers are performed. In these experiments TEWL and electrical capacitance are measured after application and removal of saline. This chapter presents pilot experiments, the experimental methodology as well as experimental results obtained.

3.1 Introduction

In order to test the quadriphasic mixture model of skin, reliable data on human subjects are required. In the past, multiple experiments have been performed in which the TEWL was measured after occlusion or application of an irritant patch. To our knowledge, measurements on TEWL after exposure of skin to an external saline (salt solution) have scarcely been reported previously [Barel & Clarys '97]. This type of measurements is adequate to test the skin model because of the well defined boundary conditions. For this reason the present chapter deals with experiments on volunteers in which TEWL will be measured following application of a solution with varying salt concentration. First a brief description of occlusion and application of saline (occlusion + hydration) is given.

Occlusion; Skin occlusion results in increased hydration of the skin because of inhibition of water evaporation [Berardesca *et al.* '92]. Hydration achieved by occlusion results in an increased TEWL when the occluding film is removed until the excessive amount of water trapped within the stratum corneum evaporates and the corneum water content reaches equilibrium with the environment [Agner & Serup '93, Berardesca & Maibach '90, Graves *et al.* '95]. TEWL measurements after occlusion quantifies the skin's water holding capabilities and is an indirect measurement of the in vivo water content [Berardesca *et al.* '92].[1] The decreasing water loss curve measured after occlusion is often expressed as skin surface water loss (SSWL), whereas transepidermal water loss (TEWL) is the baseline evaporation of water through the

[1] In normal skin higher values of TEWL indicate higher hydration levels of the stratum corneum. In scaly skin, however, there is an inverse relationship between TEWL and stratum corneum hydration state. Therefore TEWL cannot be regarded as a direct reflection of water content in the case of scaly skin [Tagami '88].

entire epidermis. When all the excess of water present in the corneum after occlusion has evaporated, SSWL equals TEWL [Berardesca & Maibach '90, Berardesca *et al.* '92].

Application of saline; When the skin is exposed to an external saline solution, it moves towards a new equilibrium. When applying distilled water, the skin saturates with water. As the skin has a physiological saline concentration of 0.154 M, the resulting adsorption force of the saline in the skin causes a fluid flow out of the environment into the skin, until an equilibrium is reached. It is to be expected that the high hydration level causes an increased TEWL after removal of the applied water. The increase of TEWL decays until the value previous to application, corresponding to a normal hydration level, is reached (see figure 3.1, curve a). Application of saline with a higher molarity than physiological saline results in an adsorption force due to saline in the patch in opposite direction which may expel water out of the skin. However, an additional adsorption force due to the skin's matrix components is present in the skin and exerts an adsorption force on water. If the adsorptive effect of the saline in the patch is less than the adsorptive effect of the solid skeleton components of skin, water flows out of the skin into the applied saline until an equilibrium is reached. After removal of the saline and thus exposure of the skin to air, the skin will be more hydrated and thus the initial TEWL will be increased (curve b or c in figure 3.1, molarity of the applied saline of curve c $>$ b).

If, on the other hand, the molarity of the applied saline is very large resulting in a higher adsorptive effect of the saline in the patch than the solid skeleton components, curve d is obtained. Water is extracted out of the skin into the applied saline. After removal of the patch, the hydration of the skin will be less and thus the initial TEWL decreased with respect to TEWL before application of the patch. The increase or decrease of TEWL is expected to diminish in time until the TEWL previous to application is attained.

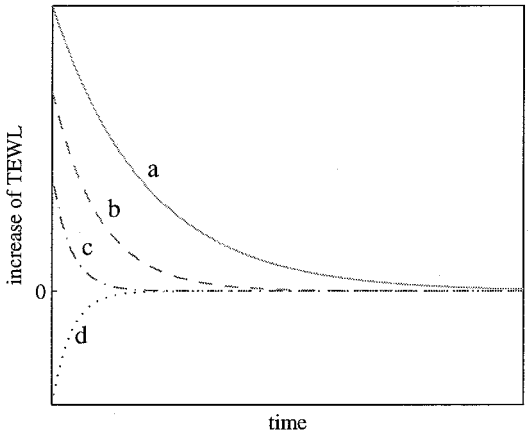

Figure 3.1: Predicted TEWL-curves as function of the molarity of the applied saline. Molarity a $<$ b $<$ c $<$ d.

3.2 Preliminary experiments

A preliminary experiment was performed to determine a suitable application time of salt solution. A set of three patches containing filters saturated with a one molarity NaCl solution was applied on the volar forearm. The patches were removed after an application time of 1, 5, and 25 hours. During the TEWL measurements the relative humidity varied between 55% and 60% and the ambient temperature was 20°C. The observed TEWL decay curves are shown in figure 3.2. The differences between the three curves are relatively small. For practical reasons, an application time of 1 hour has been chosen for the final set of experiments. The stratum corneum is assumed to be in equilibrium after 1 hour of application with saline.

In the experiment, patches (Ø 18 mm) with a height of 5 mm were attached using Leukosilk® (hypoallergenic tape of artificial silk). In a first experiment, polypropylene coated patches (Ø 18 mm) with a height of 1 mm, were attached using Leukopor® (hypoallergenic, water permeable tape). The resulting TEWL curves for the 1 hour and 5 hours application showed similar effects as displayed in figure 3.2. The 25 hours application curve, however, deviated substantially. Only a small initial increase of TEWL (less than 6 g/m^2h) was found, indicating that either the molarity of the applied solution had considerably changed or the filter had lost most of its water content and therefore was not able to hydrate the skin, or both. This phenomenon has been eliminated by using both higher patches with larger capacity and water impermeable tape.

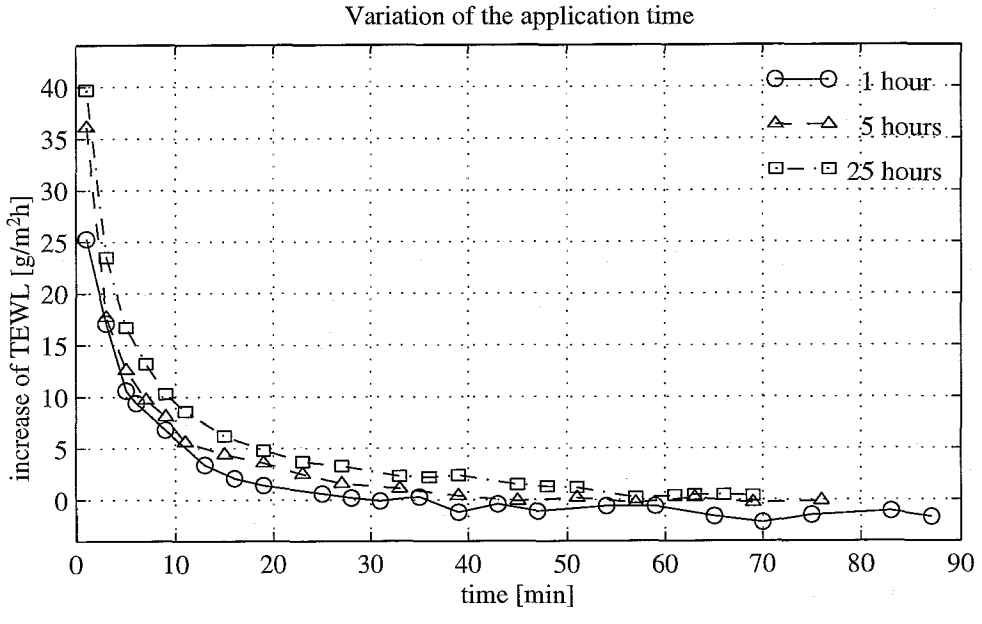

Figure 3.2: Increase of TEWL after an application time of 1 hour (circles, solid line), 5 hours (triangles, dashed line) and 25 hours (squares, dash-dotted line).

3.3 Methodology

Ten healthy volunteers (5 male and 5 female, mean age 25 with range 22–28) participated in the study. The subjects were requested not to use any skin care product on the day of the measurements. Informed consent was obtained from all participants. The study was performed in March and April of 1997 and the measurements took place in a climate room. The relative humidity varied between 50% and 60%. The room temperature was kept constant at 19-20°C. Measurements were taken on the volar forearm (both left and right arm, both dominant and non-dominant side, all with equal frequency). Subjects were preconditioned by 30 minutes of rest in the climate room.

Three areas were marked at one, two, and three quarters of the length of the volar forearm (wrist-elbow) and were not randomised with respect to the molarity of the applied saline solution. Baseline values of TEWL and capacitance were measured at these sites using the Tewameter® and Corneometer®, respectively (see section 2.2). At several points in time during the entire time-span of the experiment, TEWL and capacitance values were measured at a fourth (control) area to verify that the psychological condition of the subject was not causing an overall change of TEWL or capacitance. Three aluminium patches (height 5 mm, Ø 18 mm) were filled with filters. The filters were saturated with distilled water, 1 M NaCl solution, and 4 M NaCl solution, respectively. First a patch with 1 M saline was applied. After 20 minutes a second patch with distilled water was applied and patch number three with 4 M saline was applied another 20 minutes later. After one hour of application, the patches were removed (thus with an interval of 20 minutes) and TEWL and capacitance values were measured. The height of the patches were about four times the height of patches normally used in dermatology in order to sustain an approximately constant molarity (see section 3.2). The patches were attached using Leukosilk® with Tesa® cellulose tape on top, to ensure that neither an irritant reaction, nor water loss through the tape, occurred.

3.4 Results

3.4.1 TEWL

The measured increase of TEWL (relative to baseline values preceding application) for each subject is shown in appendix A, figure A.3. The data were fitted per subject using the least squares algorithm with an exponential regression equation of the form: increase of TEWL = $c_3 + c_2 \cdot e^{-c_1 \cdot t}$, with t the time after removal of the patch in hours. TEWL is expressed in g/m^2h, as this is the usual unit in dermatology. In figure 3.3 the measured TEWL (cross-signs) and fitted curves (solid lines) for subject 1 are displayed as example. The fit results for all subjects combined by averaging the fit parameters, are depicted in figure 3.4, with curves for 0 M (distilled water), 1 M, and 4 M NaCl solution shown in the top-left, top-right, and bottom-left panel, respectively. The bottom-right panel shows the mean curves of 0 M, 1 M, and 4 M saline combined.

Table 3.1 lists the mean and standard deviations of the estimated coefficients. In the fourth column the coefficient of determination r^2, a measure of how well the regression curve fits the data, is given. These values are visualised in appendix A, figure A.1. Normalising the TEWL data with respect to the initial increase of TEWL did not affect the variation over the subjects.

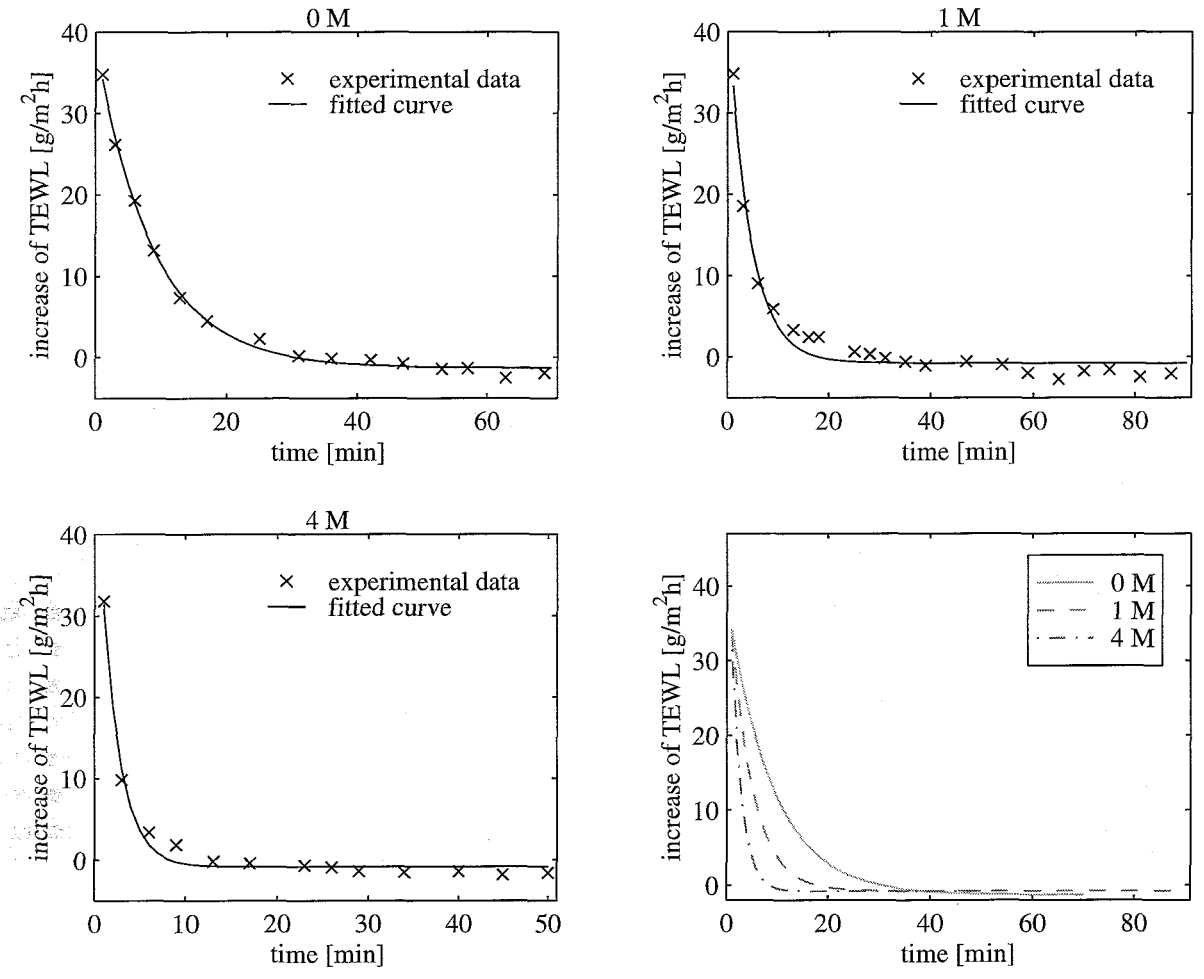

Figure 3.3: Increase of TEWL for one subject, after one hour application with distilled water (top-left panel), 1 M NaCl solution (top-right panel) and 4 M NaCl solution (bottom-left panel). Measured values are represented by cross-signs, fitted curves by solid lines. The bottom-right panel shows all three fitted curves combined: 0 M (solid line), 1 M (dashed line) and 4 M NaCl solution (dot-dashed line).

Table 3.1: Fit results of TEWL curves. Mean values ± standard deviations are listed.

Molarity	c_1 [1/h]	c_2 [g/m^{2}h]	c_3 [g/m^{2}h]	r^2 [–]
0 M	6.54 ± 1.75	43.8 ± 6.02	0.398 ± 1.09	0.991 ± 0.0066
1 M	10.9 ± 4.07	38.3 ± 8.01	0.305 ± 0.757	0.974 ± 0.0182
4 M	30.7 ± 4.33	57.1 ± 16.7	0.822 ± 0.889	0.986 ± 0.0062

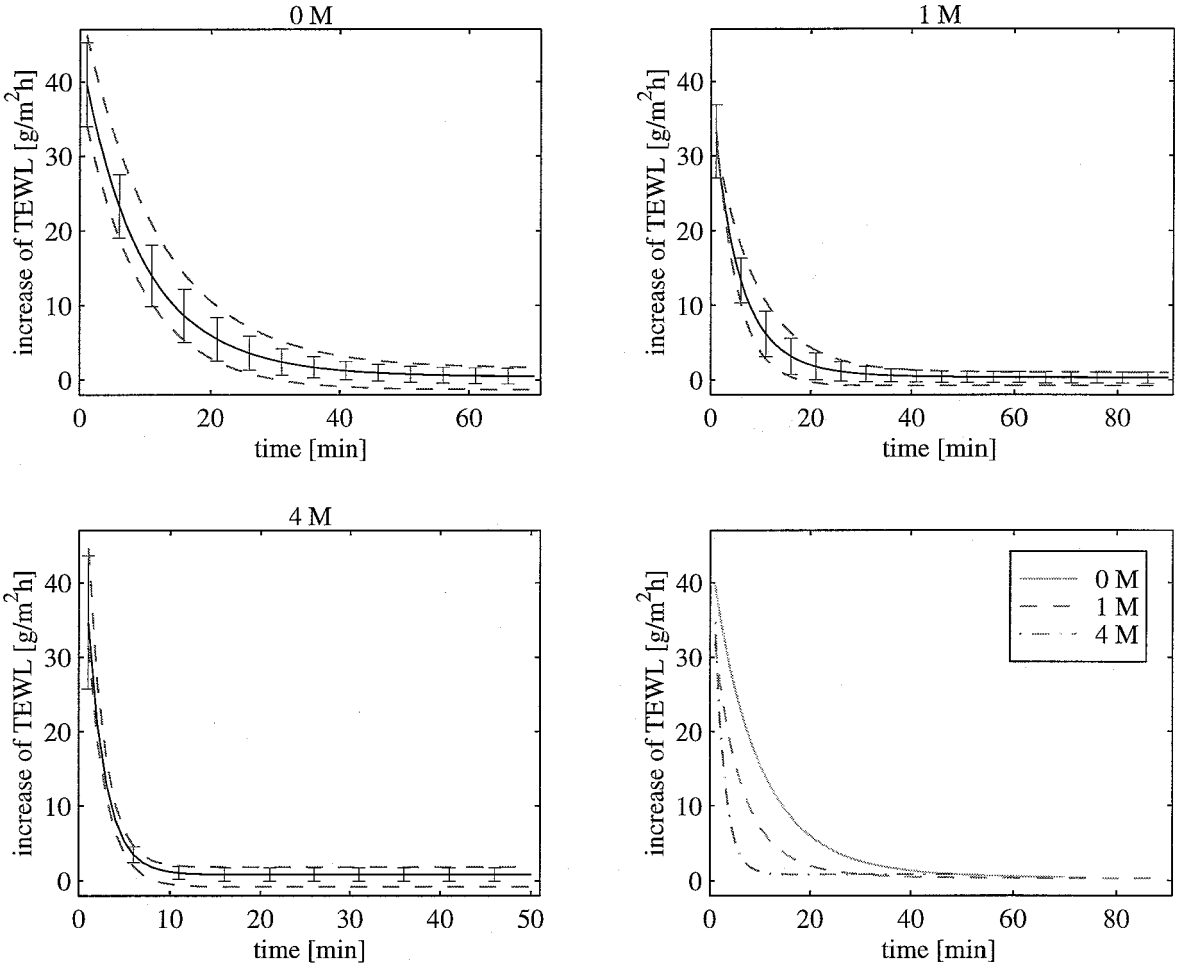

Figure 3.4: Increase of TEWL after one hour application with distilled water (top-left panel), 1 M NaCl solution (top-right panel) and 4 M NaCl solution (bottom-left panel). Fitted curves averaged over the subjects are represented by a solid line. Dashed lines show extreme curves. The standard deviation is represented by vertical bars. The bottom-right panel shows all three fitted curves combined: 0 M (solid line), 1 M (dashed line) and 4 M NaCl solution (dot-dashed line).

In table 3.2 the areas under the fitted TEWL-curves are given. These values can be regarded as the additional amount of water absorbed and accumulated under the skin during application of the patch, and thus is related to the skin's water holding capability.

Table 3.2: Mean values (μ) and standard deviations (σ) of the areas under the fitted TEWL-curves [g/m^2].

	0 M	1 M	4 M
μ	7.0583	3.8102	1.8450
σ	1.8615	0.9560	0.4140

3.4.2 Capacitance

The measured increase of electrical capacitance (relative to baseline values preceding application) are shown per subject in appendix A, figure A.4. These experimental values were fitted per subject with an exponential regression equation of the form: increase of capacitance = $d_3 + d_2 \cdot e^{-d_1 \cdot t}$, with t the time after removal of the patch in hours and the capacitance expressed in arbitrary units. In figure 3.5 the measured capacitance (markers) and fitted curves (lines) for each subject are shown.
Table 3.3 lists and figure A.2 in appendix A displays the mean values and standard deviation of the estimated coefficients d_1, d_2, and d_3 and the coefficient of determination r^2 for the capacitance curves.

Table 3.3: Fit results of capacitance-curves. Mean values ± standard deviations are listed.

Molarity	d_1 [1/h]	d_2 [a.u.]	d_3 [a.u.]	r^2 [-]
0 M	5.08 ± 2.74	24.4 ± 5.46	2.34 ± 6.32	0.977 ± 0.0153
1 M	5.62 ± 3.46	31.0 ± 9.85	1.13 ± 6.15	0.954 ± 0.0197
4 M	25.7 ± 15.0	58.5 ± 49.0	1.34 ± 4.85	0.959 ± 0.0274

Figure 3.6 shows the capacitance curves averaged over the subjects.

3.5 Discussion

According to figure 3.4 the TEWL variation over the subjects is tolerably small. This may be due to the homogeneity of the group of test persons. An exponential regression curve was able to fit the experimental data well, considering the high value of the coefficient of determination (range 0–1, higher than 0.9 for all applied salt concentrations). The initial increase of TEWL ($c_2 + c_3$ in table 3.1) is in the region of 40 g/m^{2}h. The TEWL curves decay to approximately 0 (coefficient c_3 in table 3.1), which means that the TEWL equals the baseline values preceding application of the patches. The rate of decrease depends on the molarity of the applied solution. The incline virtually has been completed after 60, 30, and 10 minutes for the 0 M, 1 M, and 4 M curve, respectively. The slope of the decay curve decreases – becomes more negative – with increasing salt concentration ensuing a more rapid

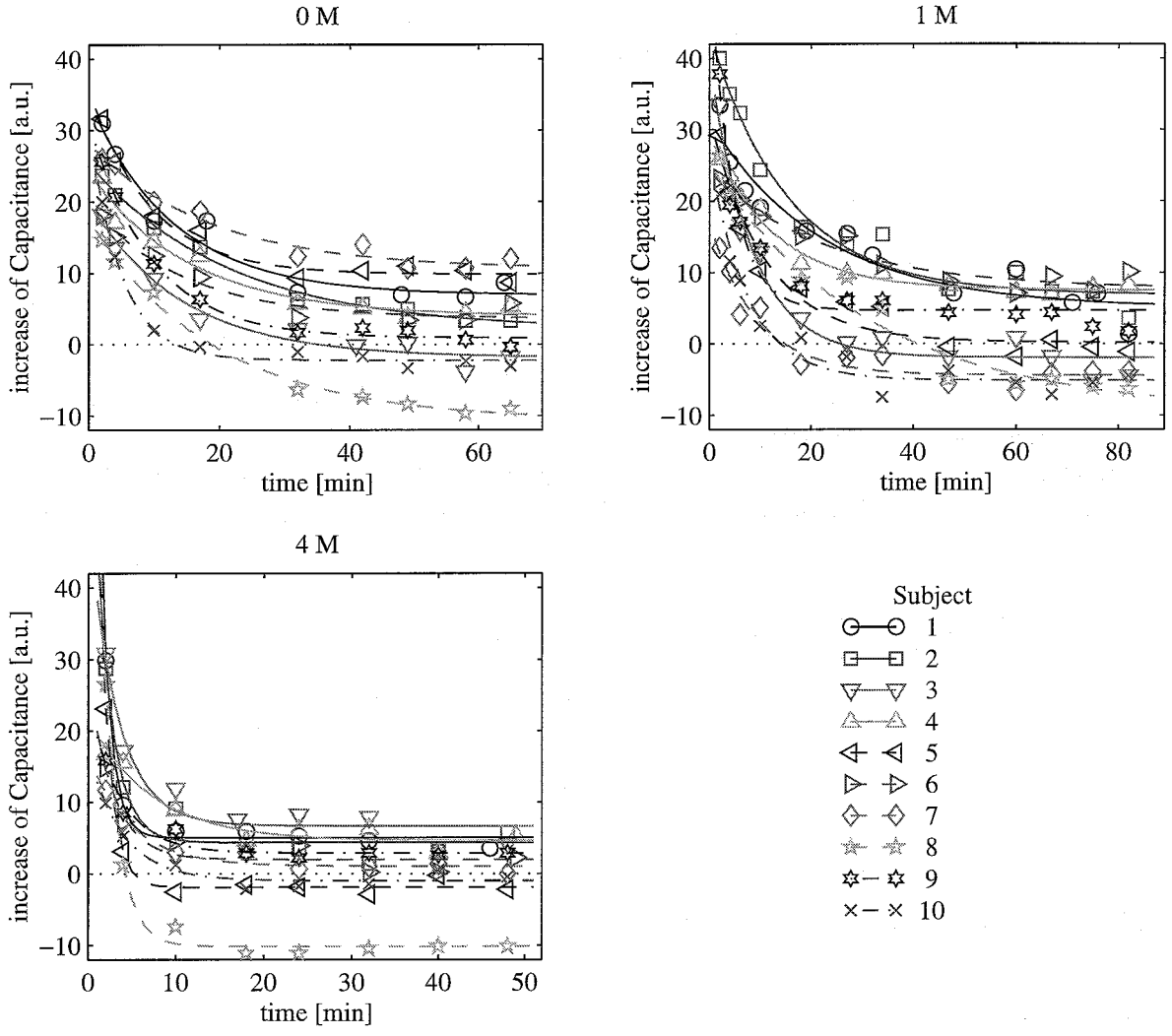

Figure 3.5: Increase of capacitance after one hour application with distilled water (top-left panel), 1 M NaCl solution (top-right panel) and 4 M NaCl solution (bottom-left panel). Measured values are represented by markers (subject dependent), fitted curves by lines.

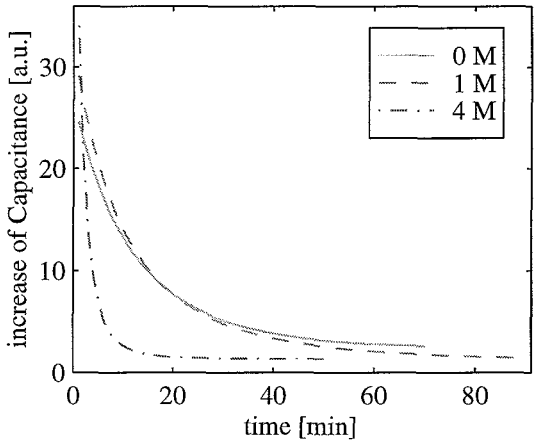

Figure 3.6: Increase of capacitance averaged over the subjects. The solid, dashed, and dot-dashed curves represent application of 0 M, 1 M, and 4 M, respectively.

recovery of equilibrium. The curves show a behaviour as predicted in figure 3.1, curves a to c, which means that the adsorptive effect of the saline in the patch is less than the adsorptive effect of the solid skeleton components. The additional amount of water accumulated under the skin (table 3.2) approximately halves when exposing the skin to saline with a molarity of 1 instead of 0 or a molarity of 4 instead of 1 M.

Figure 3.5 reflects the large variation over the subjects regarding the capacitance measurements, especially compared to the TEWL results. The data per subject were not hard to fit as indicated by the coefficient of determination, lying between 0.9 and 1.0. For most subjects, the capacitance values do not retrieve their pre-application value. The slope of the decay curves varies considerably over the subjects. No plain relation exists between the fitted curves of the three different conditions. The averaged curves per condition (figure 3.6) imply a higher initial capacitance (coefficient $d_2 + d_3$ in table 3.3) with increasing molarity of the applied solution, accompanied by a more negative initial slope ($-d_1 \cdot d_2$), ensuing a more rapid recovery of equilibrium. This behaviour differs from the observed TEWL-curves and thus is in disagreement with the expected relation between TEWL and hydration in normal skin. It is uncertain whether the measured electrical capacitance is a direct measure of hydration or a combination of hydration and ions present. It is most likely that by exposing skin to a solution with a specific salt concentration, the remaining salt at and beneath the skin surface influences the electrical skin capacitance. This would explain the higher initial capacitance with increasing molarity of the applied saline.

Chapter 4

Quadriphasic theory of the experiments

Water and ion flow in skin is simulated by using a quadriphasic mixture model for skin coupled with a diffusion model for water vapour transport in air. In this chapter a brief description of the quadriphasic mixture model – theory and finite element formulation – is given (section 4.1), as well as a diffusion model of water evaporation in air (section 4.2) and boundary conditions (section 4.3). The simulation results, obtained by combining both models with appropriate boundary conditions, are presented in section 4.5.

4.1 Quadriphasic mixture model of skin

4.1.1 Introduction

Many soils, biological tissues and gels (mineral, biological and synthetic porous media, respectively) exhibit the phenomenon of swelling and consolidation. When in contact with an external salt concentration, mobile salt ions diffuse and fluid flows between the medium and its environment until equilibrium is reached. This phenomenon is caused by a charge fixed to the solid which interacts with free charges in the fluid. Deformation of the tissue can therefore be established by either mechanical or chemical loading. The overall mechano-chemical response which occurs is the result of:

1. finite deformation due to external mechanical forces, fluid and osmotic pressure, viscosity of the fluid, and electrostatic forces,

2. relative fluid flow into or out of the tissue due to convection, Donnan osmosis, capillary forces, and surface adsorption,

3. movement of mobile ions due to diffusion, convection, and electrostatic forces.

Skin is a complex multi-component structure. It consists of a solid in which a fluid is present. The solid is mainly composed of a matrix of collagen and elastin fibres. Proteoglycans (large molecules consisting of many glycosaminoglycans linked to proteins) are entangled to the fibre matrix. Ionised carboxyl and sulphate groups attached to the proteoglycans induce a negative fixed charge. The fluid is composed of water and various molecules in solution, such as ions and nutrients.

4.1.2 Theory

In order to understand the physics of ionic and fluid flow through ionised porous media such as skin, four components are distinguished:

1. a charged solid (superscript s): the fibre network, the fixed proteoglycan ground substance, cells, and bounded water,
2. a fluid (f): mainly interstitial water,
3. cations ($+$): the small positive ions and nutrients dissolved within the fluid, treated as one positive monovalent constituent, and
4. anions($-$): the small negative ions, treated as one negative monovalent constituent.

This distinction includes fluid, ion, and electrical fluxes due to pressure, concentration, and electrical potential gradients[1]. In table 4.1 the different coupled transport phenomena in porous media are tabulated. Theoretical understanding of these phenomena in biological media subject to infinitesimal deformation has been initiated by [Lai *et al.* '91].

Table 4.1: The scope of the quadriphasic mixture model.

	pressure gradient	concentration gradient	electrical gradient
fluid flux	filtration (Darcy)	Donnan osmosis	electro-osmosis
ion flux	ultra filtration	diffusion (Fick)	electro-foresis
electrical flux	streaming current	diffusion current	conduction

In the context of this study we use finite deformation theory of charged porous media developed by [Huyghe & Janssen '97], because we expect the outer surface of the skin to exhibit larger strains in the experimental condition described in the previous chapter. They assume that

- all components are intrinsically incompressible,
- there are no (chemical) reactions between the components,
- the absolute temperature is equal for all components and is constant in time and place (isothermal),
- the volume fractions of the ions are relatively small compared to the other fractions: $n^+, n^- \ll n^s, n^f$,
- the mixture is saturated: $n^s + n^f + n^+ + n^- = 1$,
- inertial terms and body forces are negligible,

[1] In the triphasic mixture model of [Snijders *et al.* '95], the cations and anions are treated as one monovalent constituent, neglecting electrical effects. This model is able to give a good description of the swelling and consolidation phenomena of intervertebral disc tissue, but as the electrical effects are not negligible due to the high fixed charge density, a rather unrealistically high diffusion coefficient has to be chosen to fit experimental curves [Drost *et al.* '95, Frijns '96, Houben '96, Oomens '95, Snijders *et al.* '95].

Under these assumptions, a set of four coupled differential equations can be derived by combining laws of balance deduced for each component with interaction terms [Huyghe & Janssen '97]:

balance of mass of the solid and the fluid

$$\vec{\nabla} \cdot \vec{v}^s + \vec{\nabla} \cdot n^f (\vec{v}^f - \vec{v}^s) = 0, \tag{4.1}$$

balance of mass of the cations and anions

$$n^f \frac{\mathrm{D}^f}{\mathrm{D}t} \left(\frac{n^\alpha}{n^f} \right) + \vec{\nabla} \cdot [n^\alpha (\vec{v}^\alpha - \vec{v}^f)] = 0, \qquad \text{with } \alpha = +, -, \tag{4.2}$$

balance of momentum of the mixture

$$\vec{\nabla} \cdot \boldsymbol{\sigma}^{eff} - \vec{\nabla} p = \vec{0}, \tag{4.3}$$

with

$\vec{\nabla}$ = Eulerian gradient operator,
$\cdot$ = dot vector (tensor) product operator,
$\vec{v}^\alpha$ = velocity vector of the component α,
n^α = volume fraction of component α,
$\frac{\mathrm{D}^f}{\mathrm{D}t}$ = fluid material time derivative,
$\boldsymbol{\sigma}^{eff}$ = effective stress tensor, defined as $\boldsymbol{\sigma}^{eff} = \boldsymbol{\sigma} + p\boldsymbol{I}$, with $\boldsymbol{\sigma}$ = Cauchy stress tensor,
p = fluid pressure.

These equations are extended with five constitutive relationships:

elasticity

$$\boldsymbol{\sigma}^{eff} = E\boldsymbol{E}, \tag{4.4}$$

extended Darcy's law

$$n^f \vec{v}^{fs} = -\boldsymbol{K} \cdot [\vec{\nabla}_0 (p - \pi + \psi) + RT(\phi^+ \vec{\nabla}_0 c^+ + \phi^- \nabla_0 c^-) - Fc^{fc} \vec{\nabla}_0 \xi], \tag{4.5}$$

Fick's law

$$n^\alpha (\vec{v}^{\alpha s} - \vec{v}^{fs}) = -\boldsymbol{D}^\alpha \cdot \vec{\nabla}_0 \mu^\alpha, \qquad \text{with } \alpha = +, -, \tag{4.6}$$

Van't Hoff's Law

$$\pi = RT\phi^f (c^+ + c^-) + \pi_0, \tag{4.7}$$

matric potential

$$\psi = \mathcal{F}(n^f) \tag{4.8}$$

in which

E = Young's modulus,
$\boldsymbol{E}$ = Green-Lagrange strain tensor,
$\vec{v}^{\alpha s}$ = $\boldsymbol{F}^{-1} \cdot (\vec{v}^{\alpha} - \vec{v}^{s})$, flow of component α relative to solid movement, through a surface of the mixture which initially equalled a unit surface,
$\boldsymbol{F}$ = deformation tensor,
$\boldsymbol{K}$ = permeability tensor,
$\vec{\nabla}_0$ = $\boldsymbol{F}^{c} \cdot \vec{\nabla}$, Lagrangian gradient operator,
π = Donnan osmotic pressure,
π_0 = reference value of osmotic pressure,
ψ = matric potential,
ϕ^{β} = osmotic coefficient of component β,
c^{α} = concentration per unit fluid volume of component α,
F = Faraday's constant,
c^{fc} = concentration of the fixed charges in equivalent moles of univalent ions per unit volume,
$\boldsymbol{D}^{\alpha}$ = diffusion tensor of component α,
μ^{α} = electro-chemical potential of component α,
ξ = electrical potential per unit volume constituent.

Equation 4.8 expresses that the matric potential is a function of the porosity. In section 4.4 a relationship between matric potential and porosity will be derived.

The standard expression of the chemical potential of component β, per unit volume constituent, is

$$\mu^{\beta} = \mu_0^{\beta} + p + \frac{RT}{\overline{V}^{\beta}} \ln(a^{\beta}), \qquad \text{with } \beta = f, +, -, \tag{4.9}$$

with

μ_0^{β} = reference value of the chemical potential of component β,
p = fluid pressure,
R = universal gas constant,
T = absolute temperature,
$\overline{V}^{\beta}$ = partial molar volume of component β,
a^{β} = activity of component β, defined as $a^{\beta} = f^{\beta} c^{\beta}$,
with f^{β} = activity coefficient of component β,
c^{β} = concentration of component β per unit fluid volume.

The chemical potential of the fluid in the medium can be described by

$$\mu^{f} = \mu_0^{f} + p + \frac{RT}{\overline{V}^{f}} \ln(a^{f}) + \psi, \tag{4.10}$$

or, neglecting μ_0^{f},

$$\mu^{f} = p - \pi + \psi. \tag{4.11}$$

The matric potential is often neglected, but in our case where the skin is in contact with air, it plays an important role. The osmotic and matric potentials are the adsorption forces due to saline and solid skeleton components, respectively, mentioned in section 3.1. The matric potential arises from the interaction of water with the matrix of solid constituents in which

it is embedded [Marshall & Holmes '88]. Due to these attractive forces the vapour pressure above the skin is lowered compared to the water vapour pressure above pure water.

In the chemical potential equation for the cations and anions, the pressure term is negligible compared to the activity term. By adding an electrical term to account for electrical potential gradients, the resulting *electro*-chemical equations for the cations and anions are

$$\mu^+ = \mu_0^+ + \frac{1}{\overline{V}^+}(RT\ln(a^+) + F\xi), \tag{4.12}$$

$$\mu^- = \mu_0^- + \frac{1}{\overline{V}^-}(RT\ln(a^-) - F\xi). \tag{4.13}$$

4.1.3 Finite element formulation

This section represents an overall view of the finite element formulation of the quadriphasic theory. For a more elaborate mathematical description the reader is referred to [Frijns '96, Frijns *et al.* '96].

By substitution of the constitutive relationships (equations 4.4 - 4.8) into the equations of balance (equations 4.1 - 4.3), one vector and three scalar coupled differential equations are obtained. The driving forces for fluid and ion flow are proportional to the gradients of their respective chemical potentials [Richards '80]. These chemical potentials are continuous at boundaries with pressure and concentration jumps. Therefore the displacement, the chemical potential of the fluid μ^f, and the electro-chemical potential of the cations μ^+ and anions μ^- were chosen as the independent variables (degrees of freedom) for the present formulation.

The differential equations are written in an integral form using the weighted residual method. Therefore the differential equations are multiplied with arbitrarily chosen weighting functions and integrated over the current volume. Applying Gauss' theorem, some volume integrals are transformed into surface integrals. The Euler formulation is rewritten with respect to a reference state (Lagrange). The resulting equations are transformed into a finite element formulation by dividing the mixture volume into a number of elements and calculating the integrals over the total (reference) volume as the sum of integrals over these elements. Finally, the spatially discrete equations are discretised in time and solved using the Newton-Raphson iteration procedure. For the numerical simulation, a one-dimensional finite element formulation implemented in MATLAB, is used.

4.2 Diffusion model of water evaporation in air

Due to a difference in water concentration between the skin and the environment, water continuously flows from the body to the environment. The transport of water in air is given by the differential equation

$$\frac{\partial p^v}{\partial t} - \vec{\nabla} \cdot (\boldsymbol{D}^v \cdot \vec{\nabla} p^v) = 0, \tag{4.14}$$

where $\boldsymbol{D}^v$ is the diffusion tensor of water vapour in air and p^v the partial vapour pressure. Assuming the diffusion tensor independent of the position and direction, this equation can be written as

$$\dot{p}^v - D^v \vec{\nabla} \cdot \vec{\nabla} p^v = 0, \tag{4.15}$$

where $\dot{p}^v$ is the time derivative of p^v, and D^v is a scalar diffusion coefficient.

This can be written in an integral form using the weighted residual method. Therefore the differential equation is multiplied with an arbitrary weighting function h and integrated over the volume $\mathcal{V}$. By partial integration (using the chain rule for differentiation and applying Gauss' theorem) and rearranging terms, equation 4.15 is transformed into

$$\int_{\mathcal{V}} h\dot{p}^v \, dV + D^v \int_{\mathcal{V}} \vec{\nabla} p^v \cdot \vec{\nabla} h \, dV = D^v \int_{\mathcal{A}} h\vec{n} \cdot \vec{\nabla} p^v \, dA, \tag{4.16}$$

with $\mathcal{A}$ the boundary surface of the mixture and $\vec{n}$ the outward unit normal of $\mathcal{A}$.

Spatial discretisation is obtained by dividing the mixture volume in sub-volumes, the elements. The integrals over the total mixture are replaced by the sum of the integrals over the elements. Within the elements, $\mathcal{N}$ nodes are defined. Pressure p_r^v is the pressure at the r-th node ($r = 1, \ldots, \mathcal{N}$). For interpolation between the nodes, a shape function ζ_r belonging to node r, is defined. The pressure p^v is given by

$$p^v = \zeta_r p_r^v, \tag{4.17}$$

where Einstein's summation convention over the indices that appear twice, is used. The weighting function h is interpolated in the same way as p^v (Galerkin):

$$h = \zeta_s h_s. \tag{4.18}$$

Substituting equation 4.17 and 4.18 in 4.16 yields

$$\int_{\mathcal{V}} \zeta_r \zeta_s \, dV \;\; \dot{p}_r^v + D^v \int_{\mathcal{V}} \vec{\nabla}\zeta_r \cdot \vec{\nabla}\zeta_s \, dV \;\; p_r^v = D^v \int_{\mathcal{A}} \zeta_s \vec{n} \cdot \vec{\nabla} p^v \, dA. \tag{4.19}$$

Time discretisation is obtained by using the Wilson θ-method for time integration:

$$p^v = \theta p_{t+dt}^v + (1-\theta) p_t^v = \tilde{p}^v + \theta \delta p^v, \tag{4.20}$$

$$\dot{p}^v = \frac{p_{t+dt}^v - p_t^v}{dt} = \frac{\delta p^v}{dt}, \tag{4.21}$$

where θ is the time integration constant ($0 \leq \theta \leq 1$), p_t^v is the pressure at time t, dt is the time step, $\tilde{p}^v = p_t^v$, and $\delta p^v = p_{t+dt}^v - p_t^v$. Using this method, equation 4.19 can be written (in matrix notation) as

$$[\underline{M} + \theta \, dt \, \underline{K}] \;\; \underset{\sim}{\delta p}^v = dt(\underset{\sim}{Q}^{ext} - \underset{\sim}{Q}^{int}), \tag{4.22}$$

with

$$\begin{aligned}
\underline{M}_{sr} &= \int_{\mathcal{V}} \zeta_r \zeta_s \, dV, \\
\underline{K}_{sr} &= D^v \int_{\mathcal{V}} \vec{\nabla}\zeta_r \cdot \vec{\nabla}\zeta_s \, dV, \\
\underset{\sim}{Q}_s^{ext} &= D^v \int_{\mathcal{A}} \zeta_s \vec{n} \cdot \vec{\nabla} p^v \, dA, \\
\underset{\sim}{Q}_s^{int} &= D^v \int_{\mathcal{V}} \vec{\nabla}\tilde{p}^v \cdot \vec{\nabla}\zeta_s \, dV.
\end{aligned} \tag{4.23}$$

If $\theta = 0$, the method is explicit. If $0 < \theta \leq 1$, the method is implicit. Using $\theta = 1$ (Euler backward scheme) introduces a global error $\mathcal{O}(dt)$ (which can be found by Taylor-series expansion), whereas $\theta = 1/2$ (Crank-Nicolson scheme) introduces a global error $\mathcal{O}(dt^2)$. The equations derived are implemented in MATLAB in a one-dimensional form. The coupling between the quadriphasic skin model and diffusional water evaporation model will be dealt with in the next section.

4.3 Boundary conditions

The initial condition is equilibrium between the skin and an applied saline solution. Subsequently the saline is removed and the skin is exposed to air (see figure 4.1). Two layers are

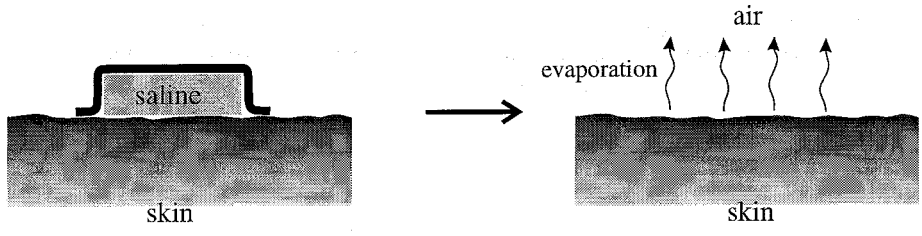

Figure 4.1: Change of skin exposure.

modelled: a skin layer consisting of the dermis and epidermis (quadriphasic mixture model) and an air layer (diffusion model). Three spatial boundaries can be distinguished: the boundary between the skin layer and the underlying tissue (dermis – hypodermis), the boundary between the skin and air (stratum corneum – air), and the boundary between the top of the air layer and the environment.

The boundary between the dermis and underlying tissue

At the bottom-side of the skin layer (epidermis and dermis), blood is present. The ion concentration of this surrounding fluid is fixed at 0.15 M. Equilibrium is described by Donnan theory, giving the concentrations at the boundary between the dermis and underlying tissue, within the dermis:

$$c^+ = \frac{1}{2}\left(-c^{fc} + \sqrt{(c^{fc})^2 + 4\left(\frac{\overline{f}^+\overline{f}^-}{f^+f^-}\right)\overline{c}^2}\right), \tag{4.24}$$

$$c^- = \frac{1}{2}\left(c^{fc} + \sqrt{(c^{fc})^2 + 4\left(\frac{\overline{f}^+\overline{f}^-}{f^+f^-}\right)\overline{c}^2}\right), \tag{4.25}$$

where overlined symbols denote values in the outer solution at the bottom side and $\overline{c} = \overline{c}^+ = \overline{c}^-$. The electrical potential of the outer solution is taken as reference, $\overline{\xi} = 0$. The boundary is permeable for both water and ions. No displacement of the boundary is assumed, so $u = 0$. The electro-chemical potentials must be continuous over the boundary:

$$\mu^\beta = \overline{\mu}^\beta, \qquad \text{with } \beta = f, +, -. \tag{4.26}$$

Combining the chemical potential equality for the fluid μ^f with the constitutive relationship for the osmotic potential π (equation 4.7) yields

$$p - \pi + \psi = -\overline{\pi} = -2RT\overline{\phi}^f \overline{c}. \tag{4.27}$$

The boundary between the stratum corneum and air

At the skin-air boundary, only water is able to evaporate from the skin to the relatively dry environment while the ions are trapped beneath the skin surface. The vapour pressure p^v just above the skin surface can be related to the chemical potential of the fluid just beneath the skin surface. Continuity of molar chemical potential at the boundary yields

$$\overline{V}^f \mu^f = \overline{V}^v \mu^v, \tag{4.28}$$

where $\overline{V}^f$ and $\overline{V}^v$ are the molar volume of the fluid and vapour, respectively, and μ^v the (volumetric) chemical potential of vapour. The molar chemical potential is used instead of the volumetric chemical potential because vapour is not incompressible [Bovendeerd & Huyghe '96]. The chemical potential of vapour can be calculated by [Marshall & Holmes '88]

$$\overline{V}^v \mu^v = RT \ln \frac{p^v}{p^v_{sat}}, \tag{4.29}$$

with p^v_{sat} the vapour pressure above pure water at skin temperature (approximately 30°C). Combination of equation 4.28 and 4.29 reveals

$$\mu^f = p - \pi + \psi = \frac{RT}{\overline{V}^f} \ln \frac{p^v}{p^v_{sat}}. \tag{4.30}$$

The fluid flux $\vec{q}^f$ leaving the top-side of the skin equals the vapour flux $\vec{q}^v$ entering the air layer at the bottom-side. These fluxes must be mass fluxes. In order to retrieve a mass flux of vapour ($D\vec{\nabla}\rho^v$, with ρ^v the vapour density), the flux given by the diffusion model of water evaporation in air described in section 4.2 ($D\vec{\nabla}p^v$), has to be multiplied by $\frac{M^v}{RT}$, where M^v is the molar mass of vapour. Figure 4.2 is a graphical representation of the coupling between the top side of the skin layer and the bottom side of the air layer.

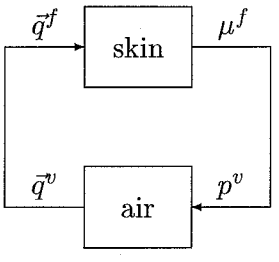

Figure 4.2: Coupling between the top side of the skin layer and the bottom side of the air layer.

By convection of water, ions are carried along and accumulated beneath the skin surface. Both the cation and anion volume flux across the boundary equals 0:

$$\vec{v}^{\alpha s} = \vec{0}, \qquad \text{with } \alpha = +, -. \tag{4.31}$$

In absence of an external mechanical force, the total stress at the boundary equals 0:

$$(\boldsymbol{\sigma}^{eff} - p\boldsymbol{I}) \cdot \vec{n} = \vec{0}. \tag{4.32}$$

The top boundary of the air layer

At 13 mm above the surface of a salt solution, the vapour pressure p^v equals the environmental pressure p^v_{env} [Nilsson '77]. p^v_{env} can be calculated by $p^v_{env} = \frac{rh}{100} \cdot p^v_{sat}$ (equation 2.2) resulting in $p^v_{env} = 1.25$ kPa ($rh = 55$ %, $T = 19.5°$C).

Initial conditions

At first, the skin is exposed to saline. The initial ion concentrations and pressure beneath the skin surface equal the concentrations and pressure given by Donnan theory (equations 4.24–4.27) when exposing to an outer solution with a specific molarity (either 0 M, 1 M, or 4 M in the experiments performed).

At a specific point in time, the applied saline is removed and the skin is exposed to air. Initially, the vapour pressure throughout the air layer equals the environmental pressure: $p^v = p^v_{env}$.

4.4 Finite element simulation set-up

The one-dimensional finite element models with described boundary conditions are implemented in MATLAB. The degrees of freedom for the quadriphasic mixture model of skin are the displacement, the chemical potential of the fluid and the electro-chemical potential of the cations and anions. The degree of freedom for the diffusion model of water evaporation in air is the vapour pressure. The shape functions are linear. The skin layer is divided into 38 elements by first dividing the layer into 30 equal parts, then dividing the last part into 10 new equal parts, and finally dividing the new last part into 10 elements. An initial thickness of 2 mm is chosen, which approximates the thickness of the epidermis and dermis. Thus the skin is constructed by successively 19, 9, and 10 elements with a height of 100 μm, 10 μm, and 1 μm, respectively. The elements near the skin surface are chosen smaller because of the large gradients in the degrees of freedom and material parameters.

The air layer is divided into 5 equivalent elements and its total thickness is 13 mm. The time step is 100 s. Initially the time integration constant θ is 1 [-]. For subsequent increments a time integration constant of 0.6 is used. The molarity of the applied saline solution is 1 M. At the bottom side a molarity of 0.15 M is prescribed.

The material parameters are not uniform in space (due to the presence of different layers) and time (due to deformation of the skin). Spatial variety of properties is obtained by initial profiles of the material parameters whereas temporal variety is obtained by deformation dependent relationships as presented below. The hydro-lipid film at the surface of the skin is not modelled.

Porosity

The porosity n^f (water volume fraction) varies over the depth in the skin. [Hansen & Yellin '72] showed that there are three different types of water present in the human stratum corneum:

1. primary water which is bound at polar sites of protein,
2. secondary water which is less tightly bound with hydrogen bonds to the primary water,
3. 'bulk' or 'free' water.

Based on experiments of [Anderson *et al.* '73] it is assumed that the 'bulk' water is located primarily intracellular and is part of the solid, whereas the primary and secondary water is located intercellular and is related to the porosity. [Warner *et al.* '88] measured the total water content of human skin as function of the depth in the skin. These values are divided into intercellular and intracellular water content by usage of the fraction primary, secondary and 'bulk' water as function of total water content, measured by [Hansen & Yellin '72]. A fit of the intercellular water content is used as initial porosity n_0^f [-]:

$$n_0^f = 0.3551 - \frac{1}{(2.1163 \cdot 10^4 x + 1.1548)^{10.9953}}, \tag{4.33}$$

where x is the distance to the surface of the skin [m]. Rewriting the relation of the relative volume change

$$J = \frac{1 - n_0^f}{1 - n^f}, \tag{4.34}$$

yields the momentary porosity dependent on the deformation:

$$n^f = 1 - \frac{1 - n_0^f}{J}. \tag{4.35}$$

Fixed charge density

Hardly any data are available on the fixed charge density of skin. Based on experiments by Van Kemenade (personal communication), the initial fixed charge density c_0^{fc} is chosen 0.015 M throughout the thickness of the skin. It was not possible to measure a fixed charge density profile in these experiments, so the fixed charge density may be higher in the stratum corneum with respect to the underlying living tissue. The fixed charge density varies with the skin's deformation. The fixed charge density in deformed state is expressed by

$$c^{fc} = \frac{n_0^f c_0^{fc}}{n_0^f - 1 + J}. \tag{4.36}$$

Young's modulus

[Park & Baddiel '72] measured the Young's modulus E [N/m^2] as function of the ambient relative humidity rh [-]. For this purpose uniaxial tensile tests parallel to the skin surface were performed on pig skin in equilibrium with the relative humidity rh. A fit of these results is given by

$$E = 0.84 e^{-(\frac{rh}{100} + 0.5022)^{4.8002} + 22.0003)}. \tag{4.37}$$

A fit of the relative humidity as function of the porosity n^f, in equilibrium, resulting from a combination of literature data ([Anderson *et al.* '73, El-Shimi & Princen '78, Spencer *et al.* '75]), is given by

$$\frac{rh}{100} = e^{(7.0311 \cdot 10^2 (e^{9.7 \cdot 10^{-5}} - e^{\frac{9.7 \cdot 10^{-5}}{n^f}})}. \tag{4.38}$$

Substituting this relation in equation 4.37 yields

$$E = 0.84e^{-(e^{7.0311\cdot10^2(e^{9.7\cdot10^{-5}}-e^{\frac{9.7\cdot10^{-5}}{n^f}})+0.5022)^{4.8002}+22.0003)}}. \tag{4.39}$$

This equation represents the in-plane relative stiffness of stratum corneum. No data are available for stiffness perpendicular to the plane. To realise numerical convergence, equation 4.39 is multiplied by 2.
In the experiments of [Park & Baddiel '72] the Young's modulus is measured by incremental change of the applied load,

$$E(n^f) = \frac{\partial\sigma}{\partial\epsilon}. \tag{4.40}$$

In the one-dimensional situation that we consider, the strain is directly coupled to the porosity. Therefore the effective stress is calculated by

$$\sigma^{eff} = \int_0^{\epsilon} E(n^f)\mathrm{d}\epsilon = \int_{n_0^f}^{n^f} E(n^f)\frac{\partial\epsilon}{\partial n^f}\mathrm{d}n^f. \tag{4.41}$$

Figure 4.3 shows the effective stress as function of the porosity.

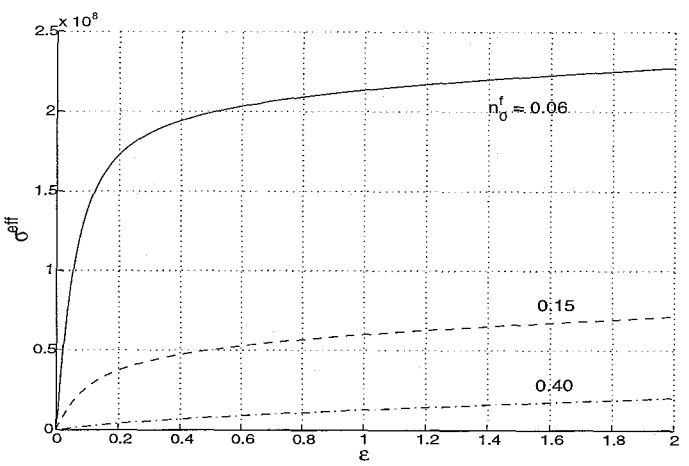

Figure 4.3: Effective stress as function of strain for several initial porosities.

Permeability

[Van Andel '97] measured in vitro the permeability of rat skin by hydration of both sides of the skin sample. She found a value in the order of 10^{-14} [m^4/Ns]. Unlike the in vitro permeability measured by Van Andel, the in vivo permeability is not the same throughout the thickness of the skin and is much lower near the surface, where the water fraction is very low [Warner *et al.* '88]. Based on the measurements of van Andel, a constant value of the initial permeability K_0 of $1 \cdot 10^{-14}$ [m^4/Ns] is assumed in the dermis. A permeability profile in the epidermis is assumed, with a value of $K_0 = 5 \cdot 10^{-24}$ at the surface of the skin. This very low value of permeability is dictated by mass balance of the fluid across the stratum corneum and the very steep gradient of matric potential. Combination of the permeability

profile and the porosity profile results in K as function of the porosity n^f. Substitution of equation 4.35 yields an expression of K as function of the initial permeability profile K_0, the initial porosity n_0^f and the volume change quotient J:

$$K = K_0 \cdot e^{21.5782(1-n_0^f)(1-\frac{1}{J})}. \tag{4.42}$$

Diffusion

The diffusion coefficients of the ions, D^+ and D^-, depend on the porosity n^f and temperature T. For simplicity a constant value (based on $n^f = 0.4$ and $T = 25°$ C) of $1.0 \cdot 10^{-10}$ [m^2/Ns] is taken for both the cations and anions [Maroudas '88].

Matric potential

[Anderson *et al.* '73, El-Shimi & Princen '78, Spencer *et al.* '75] measured the water content of skin as function of the relative humidity of the environment. As the measurements were performed in equilibrium, the vapour pressure at the surface of the skin equals the environmental vapour pressure. The vapour pressure at the surface of the skin is transformed into the chemical potential of the fluid using equation 4.30. A fit is given by

$$\mu^f = 9.84 \cdot 10^{10} \, (e^{9.7 \cdot 10^{-5}} - e^{\frac{9.7 \cdot 10^{-5}}{n^f}}). \tag{4.43}$$

Balance of momentum at the surface requires:

$$\sigma = \sigma^{eff} - p = 0. \tag{4.44}$$

The effective stress is given by the non-linear relationships shown in figure 4.3. Within the range of strains that we consider, this non-linear behaviour can reasonably be linearised. Therefore

$$p = \sigma^{eff} = \frac{E}{1+\nu}\left[\boldsymbol{E} + \frac{\nu}{1-2\nu}\mathrm{tr}(\boldsymbol{E})\boldsymbol{I}\right], \tag{4.45}$$

where ν is the Poisson's ratio with a value of 0.40 [-] and E is given by equation 4.37. With the assumption of three-dimensional homogeneous deformation ($E_{11} = E_{22} = E_{33} = \epsilon$) in this experiment, the equation is transformed into

$$p = \frac{E}{1-2\nu}\epsilon, \tag{4.46}$$

where ϵ is the strain and equals $\frac{1}{2}(\lambda^2 - 1)$, with λ the elongation factor. The relative volume change J equals λ^3. By substitution of the relation for the relative volume change (equation 4.34), equation 4.46 can be written as

$$p = \frac{E}{2(1-2\nu)}\left(\left(\frac{1-\breve{n}_0^f}{1-n^f}\right)^{2/3} - 1\right), \tag{4.47}$$

where $\breve{n}_0^f$ is the porosity in stress free state, chosen 0.05 [-]. Combining the standard equation for the chemical potential of the fluid, $\mu^f = p - \pi + \psi$ (equation 4.11), with equation 4.43 and 4.47 results in an expression for ψ [N/m^2]:

$$\psi = 9.84 \cdot 10^{10} \, (e^{9.7 \cdot 10^{-5}} - e^{\frac{9.7 \cdot 10^{-5}}{n^f}}) - \frac{E}{2(1-2\nu)}\left\{\left(\frac{1-\breve{n}_0^f}{1-n^f}\right)^{\frac{2}{3}} - 1\right\} + \pi. \tag{4.48}$$

4.5 Results

First the skin is exposed to a 1 M saline solution. The concentrations of 1 M on top of the skin, and 0.15 M at the bottom, were prescribed. The initial chemical potentials at the inner nodes, were interpolated values between these boundary conditions. Subsequently, the model was allowed to move to a steady state situation.

In figure 4.4 the numerical results are visualised. Different shades of gray denote different depths in the skin; depth 0 mm (light gray) represents the node at the surface, whereas depth 2 mm in underformed state (black) represents the node at the boundary between the dermis and hypodermis. The top left, top right, bottom left, and bottom right panel show the displacement, chemical potential of the fluid, concentration of the cations, and the fluid flow (g/m^2h), respectively.

The skin swells considerably due to water inflow at the bottom side. This results in a dynamic equilibrium in which the (small amount of) water inflow at the top side (outer boundary of the skin) equals the water outflow at the bottom side (inner boundary between the dermis and hypodermis). The skin has reached a constant height and is strained. Initially the ion concentrations slightly rise due to convection, but as the water flow decreases to a small value, a linear ion concentration profile develops.

At $t = 100$ min, the saline boundary condition is substituted by the air layer. The concentration decreases because of the absence of the concentration condition of 1 M at the top side of the skin. The fluid flow at the top side reveals a TEWL of about 90 g/m^2h, constant in time. This is approximately twice as much as the initial TEWL observed in the experiments.

Figure 4.5 shows the results of a similar simulation with this difference that at the bottom side (boundary between the dermis and hypodermis) the permeability is lowered to $1 \cdot 10^{-20}$ [m^4/Ns] to take into account a limited fluid flow as will be described in section 4.6.

In the hydration part, the height increases less rapidly due to the limited inflow at the bottom side. After substitution of saline by air (at $t = 100$ min), the concentration rapidly decreases. The skin shrinks. TEWL decreases slightly from 96 to 73 [g/m^2h]. The chemical potential of the fluid becomes positive and then goes down to negative values.

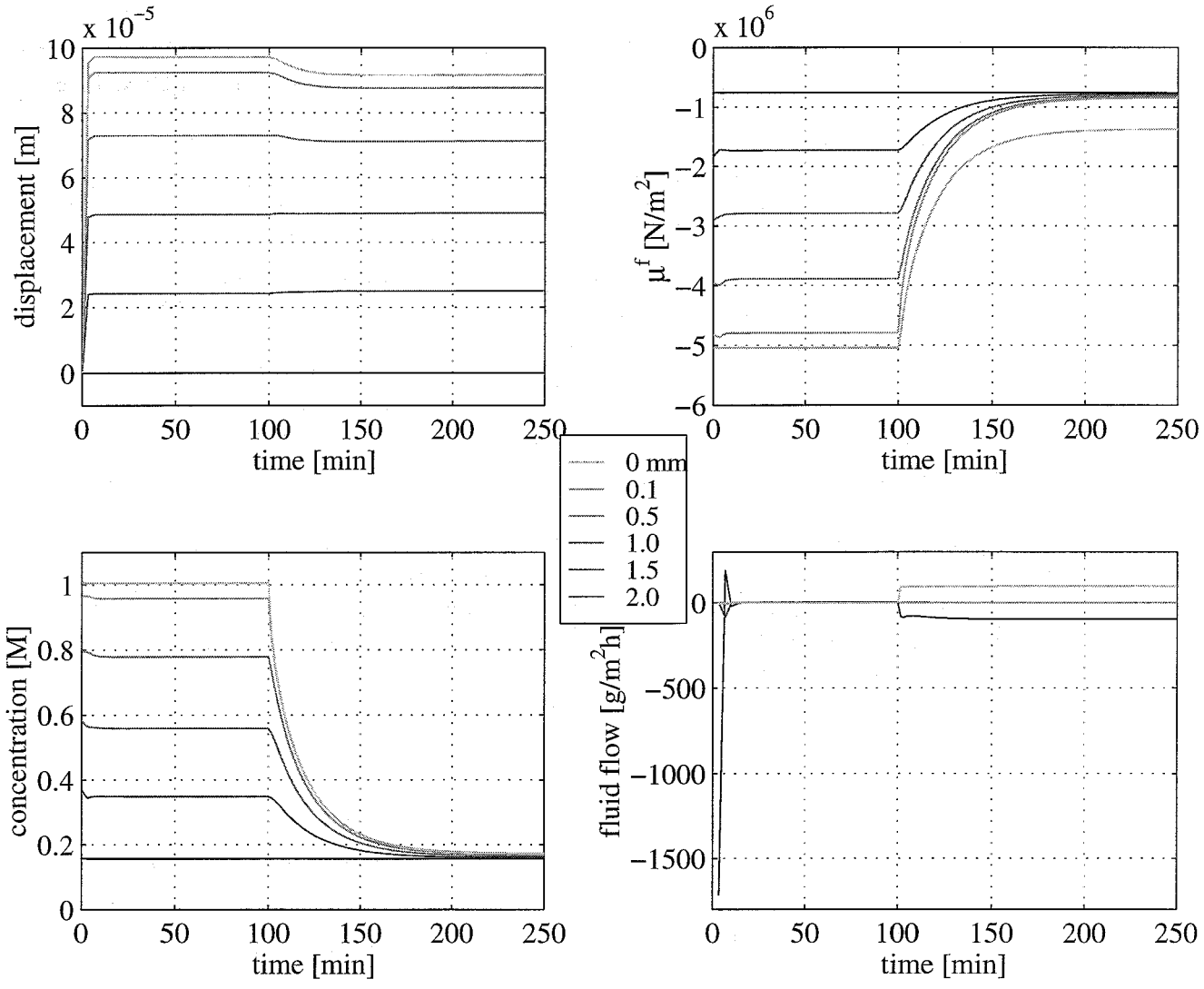

Figure 4.4: Numerical results. Different depths in the skin are denoted by different shades of gray. The top left, top right, bottom left, and bottom right panel show the displacement, chemical potential of the fluid, concentration of the cations, and the fluid flow (g/m^2h), respectively.

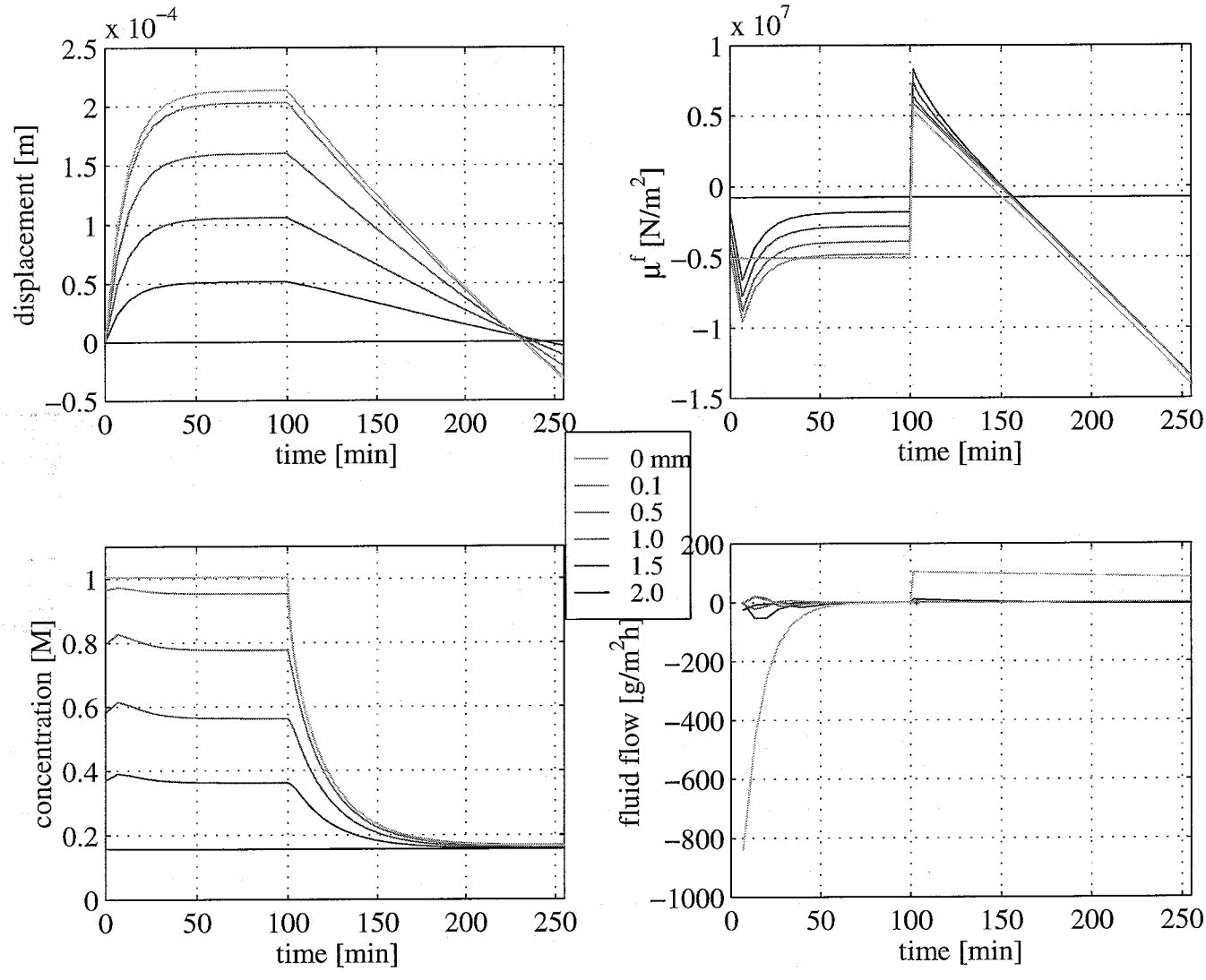

Figure 4.5: Numerical results whith lowered permeability at the boundary between dermis and hypodermis. Different depths in the skin are denoted by different shades of gray. The top left, top right, bottom left, and bottom right panel show the displacement, chemical potential of the fluid, concentration of the cations, and the fluid flow (g/m^2h), respectively.

4.6 Discussion

In this study two consecutive stages of the experiment were simulated: the hydration stage and the evaporation stage. The simulation of the hydration stage, cannot be compared to experimental results. The resulting hydration curves and concentration curves seem to reflect the expected physiological responses. A linear concentration profile develops and the skin swells. When the hydrated skin is exposed to air, the displacements and concentrations respond as expected. The skin shrinks and TEWL peaks to 90 g/m^{2}h. However, the fluid flow is higher than observed in the experiments and remains almost constant in time. The differences between measured and calculated fluid flow may be due to the following:

- The amount of fluid entering the skin at the bottom side (boundary between the dermis and hypodermis) is restricted due to limited capillary filtration. The amount of fluid filtration is [Guyton & Hall '96]:

$$0.01 \left[\frac{\text{ml}}{\text{min} \cdot \text{mm Hg} \cdot 100 \text{ g tissue}} \right].$$

  The average pressure difference over a capillary wall is 0.3 mm Hg. The average weight of an adult is about 70 kg. These data yield a fluid filtration of the entire body of 2.1 ml/min. Assuming a total body surface of 2 m^2, the maximum fluid inflow at the dermis–hypodermis boundary is 63 g/m^{2}h. This implies that when in dynamic equilibrium (outflow at stratum corneum equals inflow at dermis) the TEWL is limited to approximately 60 g/m^{2}h. Therefore a simulation is performed in which the permeability at the bottom side is considerably decreased (figure 4.5).

  A positive chemical potential at the surface of the skin indicates that the vapour pressure is higher than the saturated vapour pressure (equation 4.30). This implies that condensation occurs at the surface. This effect is not implemented in the numerical model.

- The area under the experimental TEWL-curve after application of a saline solution of 1 M, is approximately 3.8 [g/m^2] (table 3.2). Conversion of masses to volumes yields $3.8 \cdot 10^{-6}$ [m^3/m^2]. This means that if the additional amount of water that evaporates after exposure to water, was stored within the skin, the height of the skin was increased by 3.8 [μm]. As the thickness of the stratum corneum is approximately 15 [μm], it is hypothesised that this additional amount of water is stored in the stratum corneum, which will be swollen up to one and a half times its original height. [Blank '52] stated that the rapid decrease of water loss after hydration implies that the main barrier against water loss is situated deeper in the skin. A way to model this hypothesis is to shift the low permeability from the very surface of the skin towards the boundary between the stratum corneum and the underlying tissue.

- Water may flow in and out of the cells, changing the amount of intercellular fluid. It is even possible that the keratinocytes play an active role by means of distribution of ions when exposed to an unusual mechanical, chemical, or electrical load.

- The hydro-lipid film at the surface of the skin is not modelled. This waterproof layer may result in a decreased attraction of water when exposing skin to water or saline solution. The absence of this layer in the simulations may be responsible for a higher calculated TEWL with respect to the experiments.

- The literature values of the material parameters lie within a wide range of values. The values used for the simulations can be chosen arbitrary within that range. Moreover, the parameters are not the same throughout the skin. Particularly the stratum corneum has different properties. Therefore reliable data from experiments in which material parameters are measured as function of the depth and the deformation of skin are needed.

During the simulations, severe convergence problems and long computation times were encountered. Possible numerical problems are:

- The element Peclet number, $Pe = \frac{|\vec{v}|h}{D}$, ventures in a critical range. To ensure a number of Peclet less than one, the diffusion coefficient D can be chosen higher, the time step smaller or the height h of the elements smaller. If the element Peclet number is greater than 1, the convection dominates over the diffusion and the strong change of the degrees of freedom over short distance near the boundary results in oscillations so strong that the iterative solver fails to converge.

- By using linear shape functions in the elements, a linear profile of the degrees of freedom is forced. This can be overcome by using more elements, with as a result even longer computation times than already encountered.

- The time step should be larger than $\frac{h^2}{D}$ and $\frac{h^2}{KE}$, otherwise the change of the degrees of freedom in the elements seems to be absent with convergence problems as a result. If the time step is chosen too small, severe oscillations occur. Furthermore, because D and KE differ in magnitude and KE also differs along elements, it is difficult to find the appropriate time step.

- Both the variation of the material parameters over the depth – for example, the permeability varies over 10 decades – and the tremendous change of independent variables makes great demands on the numerical implementation. The large variation of the material parameters results in a badly conditioned system matrix. The values of the independent variables at the boundaries considerably change in time.

Chapter 5

Conclusions and recommendations

5.1 Conclusions

- According to the experiments, TEWL increases after application of water or a salt solution of either 1 M or 4 M. The higher TEWL decreases exponentially until pre-application values are obtained. With increasing molarity TEWL reaches these values more rapidly.
- The electrical capacitance as measured with the Corneometer shows a large variation over the subjects and does not retrieve pre-application value. It is uncertain whether the measured capacitance is a correct measure of hydration under these experimental circumstances.
- For the simulation of hydration of the skin, reasonable results are obtained. When the hydrated skin is exposed to air, the displacements and concentrations respond as expected. The calculated fluid flow is higher than experimentally observed and almost constant in time. This may be due to the existence of a second unmodelled barrier at the boundary between the dermis and hypodermis or due to a shift in the barrier at the surface of the skin.

5.2 Recommendations

- To gain more realistic simulations, material parameters as function of the depth to the surface and the deformation of skin need to be used. Depth and deformation dependent relationships are already implemented for most parameters, but not as accurate as desired.
- New measuring methods are needed to enable measuring of the profile of material parameters, eg. permeability and Young's modulus, with a resolution in the order of magnitude of one μm.
- Implementation of the relationships makes great demands on the numerical method, because of the critical domain of degrees of freedom (e.g. large Peclet number).
- As the calculation time is already enormous, it is advisable to change to a more efficient package (probably with loss of flexibility) or to use more efficient algorithms.

- Expansion of the program from the one-dimensional form to a three-dimensional implementation (either in Matlab or in another package) is desirable when simulating damaged skin.
- It is doubtful whether the measured capacitance values are a correct measure of hydration level after exposure to a saline solution. To quantify the hydration of skin in vivo, a different measuring device should be developed or searched for.

Bibliography

[Agner & Serup '93] T. Agner, J. Serup,
Time course of occlusive effects on skin evaluated by measurement of transepidermal water loss (TEWL). *Contact Dermatitis*, **28**, 6–9, 1993

[Van Andel '97] C.J. van Andel,
Bepaling van de permeabiliteit van rattenhuid. Technical report (WFW-rapport 97.042), Eindhoven University of Technology, Eindhoven, The Netherlands, 1997

[Anderson *et al.* '73] R.L. Anderson, J.M. Cassidy, J.R. Hansen, W. Yellin,
Hydration of stratum corneum. *Biopolymers*, **12**, 2789–2802, 1973

[Barel & Clarys '95] A.O. Barel, P. Clarys,
Study of the stratum corneum barrier function by transepidermal water loss measurements: Comparison between two commercial instruments: Evaporimeter® and Tewameter®. *Skin Pharmacology*, **8**, 186–195, 1995

[Barel & Clarys '97] A.O. Barel, P. Clarys,
In vitro calibration of the capacitance method (Corneometer CM 825) and conductance method (Skicon-200) for the evaluation of the hydration state of the skin. *Skin Research and Technology*, **3**, 107–113, 1997

[Berardesca & Maibach '90] E. Berardesca, H.I. Maibach,
Monitoring the water-holding capacity in visually non-irritated skin by plastic stress test (POST). *Clinical and Experimental Dermatology*, **15**, 107–110, 1990

[Berardesca *et al.* '92] E. Berardesca, G. P. Vignoli, D. Fideli, H. Maibach,
Effect of occlusive dressings on the stratum corneum water holding capacity. *American J. Medical Sciences*, **304**, 25–28, 1992

[Berardesca '97] E. Berardesca
EEMCO guidance for the assessment of stratum corneum hydration: electrical methods. *Skin Research and Technology*, **3**, 126–132, 1997

[Blank '52] I.H. Blank,
Factors which influence the water content of the stratum corneum. *J. Investigative Dermatology*, **18**, 433–440, 1952

[Blichmann & Serup '88] C.W. Blichmann, J. Serup,
Assessment of skin moisture. Measurement of electrical conductance, capacitance and transepidermal water loss. *Acta Dermato-Venereologica (Stockholm)*, **68**, 284–290, 1988.

[Bovendeerd & Huyghe '96] P.H.M. Bovendeerd, J.M.J.R. Huyghe,
Tissue mechanics, Dictaat bij college no. 4J020, Eindhoven University of Technology, Eindhoven, The Netherlands, 1996

[Drost *et al.* '95] M.R. Drost, P. Willems, H. Snijders, J.M. Huyghe, J.D. Janssen, A. Huson, Confined compression of canine annulus fibrosus under chemical and mechanical loading. *J. Biomechanical Engineering, transactions of the ASME*, **117**, 390–396, 1995

[El-Shimi & Princen '78] A.F. El-Shimi, H.M. Princen,
Water vapor sorption and desorption behavior of some keratins. *Colloid & Polymer Science*, **256**, 105–114, 1978

[Frijns '96] A.J.H. Frijns,
Vierfasenmechanica van zwellende poreuze media, Master of Science Thesis, no. WFW 96.060, Eindhoven University of Technology, Eindhoven, The Netherlands, 1996

[Frijns *et al.* '96] A.J.H. Frijns, J.M. Huyghe, J.D. Janssen,
A validation of the quadriphasic mixture theory for intervertebral disc tissue, RANA: reports on applied and numerical analysis, no. 9622, Eindhoven University of Technology, Eindhoven, The Netherlands, 1996

[Graves *et al.* '95] C.J. Graves, C. Edwards, R. Marks,
The effects of protective occlusive gloves on stratum corneum barrier properties. *Contact Dermatitis*, **33**, 183–187, 1995

[Guyton & Hall '96] A.C. Guyton, J.E. Hall,
Textbook of medical physiology. 9th ed., W.B. Saunders Company, Philadelphia, 1996

[Hansen & Yellin '72] J.R. Hansen, W. Yellin
NMR and infrared spectroscopic studies of stratum corneum hydration. *Water structure at the water-polymer interface*, ed. by H.H.G. Jellinek, Plenum Press New York, 1972

[Hattingh '72] J. Hattingh,
The influence of the skin temperature, environmental temperature and relative humidity on transepidermal water loss. *Acta Dermato-Venereologica (Stockholm)*, **52**, 438–440, 1972

[Houben '96] G.B. Houben,
Swelling and compression of intervertebral disc tissue: model and experiment, Ph.D. thesis, Eindhoven University of Technology, Eindhoven, The Netherlands, 1996

[Huyghe & Janssen '97] J.M. Huyghe, J.D. Janssen,
Quadriphasic mechanics of swelling incompressible porous media. *International J. Engineering Science*, **35**, no. 8, 793–802, 1997

[Van Kemenade *et al.* '97] P.M. van Kemenade, J.M. Huyghe, L.F.A. Douven,
Not viscous drag but matric forces are responsible for skin barrier function. In: 1997 Advances in Bioengineering, ed. by B. Simon, American Society of Mechanical Engineers, New York, 1997

[Lai *et al.* '91] W.M. Lai, J.S. Hou, V.C. Mow,
A triphasic theory for the swelling and deformation between behaviours of articular cartilage. *J. Biomech. Eng.*, **113**, 245–258, 1991

[Maroudas '88] A. Maroudas,
Nutrition and metabolism of the intervertebral disc. *The biology of the intervertebral disc, vol. 2*, Chap. 9, ed. by P. Ghosh, CRC Press, Boca Raton, 1988

[Marshall & Holmes '88] T.J. Marshall, J.W. Holmes
Soil physics, 2nd ed., Cambridge University Press, 1988

[Nilsson '77] G.E. Nilsson,
Measurement of water exchange through skin. *Medical and Biological Engineering and Computing*, **15**, 209–218, 1977

[Ollmar & Emtestam '92] S. Ollmar, L. Emtestam,
Electrical impedance applied to non-invasive detection of irritation in skin. *Contact Dermatitis*, **27**, 37–42, 1992

[Oomens '95] C.W.J. Oomens, H.J. De Heus, J.M. Huyghe, L. Nelissen, and J.D. Janssen,
Validation of the triphasic mixture theory for a mimic of intervertebral disk tissue. *Biomimetics*, **3**, no. 4, 171–185, 1995

[Park & Baddiel '72] A.C. Park, C.B. Baddiel,
Rheology of stratum corneum-II: A physico-chemical investigation of factors influencing the water content of the corneum. *J. Soc. Cosmet. Chem.*, **23**, 12–21, 1972

[Pinnagoda *et al.* '90] J. Pinnagoda, R.A. Tupker, T. Agner, J. Serup,
Guidelines for transepidermal water loss (TEWL) measurement. *Contact Dermatitis*, **22**, 164–178, 1990

[Richards '80] E.G.Richards,
An introduction to physical properties of large molecules in solution Cambridge University Press, Cambridge, UK, 1980

[Snijders *et al.* '95] H. Snijders, J.M. Huyghe, J.D. Janssen,
Triphasic finite element model for swelling porous media. *International J. Numerical Methods in Fluids*, **20**, 1039–1046, 1995

[Spencer *et al.* '75] T.S. Spencer, C.E. Linamen, W.A. Akers, H.E. Jones,
Temperature dependence of water content of stratum corneum. *Br. J. Dermatology*, **93**, 159–164, 1975

[Stender *et al.* '90] I.M. Stender, C. Blichmann, J. Serup,
Effects of oil and water baths on the hydration state of the epidermis. *Clinical and Experimental Dermatology*, **15**, 206–209, 1990

[Tagami *et al.* '80] H. Tagami, M. Ohi, K Iwatsuki, Y. Kanamaru, M. Yamada, B. Ichijo,
Evaluation of the skin surface hydration in vivo by electrical measurement. *J. Investigative Dermatology*, **75**, 500–507, 1980

[Tagami *et al.* '82] H. Tagami, Y. Kanamaru, K. Inoue, S. Suehisa, F. Inoue, K. Iwatsuki, K. Yoshikuni, M. Yamada,
Water sorption-desorption test of the skin in vivo for functional assessment of the stratum corneum. *J. Investigative Dermatology*, **78**, 425–428, 1982

[Tagami '82] H. Tagami,
Electrical measurement of the water content of the skin surface. *Cosmetics & Toiletries*, **97**, 39–47, 1982

[Tagami '88] H. Tagami,
Impedance measurement for evaluation of the hydration state of the skin surface. In: *Cutaneous investigation in health and disease, noninvasive methods and instrumentation*, Chap. 5, 79–111, ed. by J.L. Lévêque, Marcel Dekker, New York, 1988

[Thiele & Malten '73] F.A.J. Thiele, K.E. Malten,
Skin resistance measurements with alternating current (impedance measurements). *British J. Dermatology*, **89**, 373–382, 1973

[Warner *et al.* '88] R.R. Warner, C. Mark, B.S. Meyers, D.A. Taylor
Electron probe analysis of human skin: determination of the water concentration profile. *J. Investigative Dermatology*, **90**, 218–224, 1988

[Zuang *et al.* '97] V. Zuang, C. Rona, F. Distante, E. Berardesca,
The use of a capacitance device to evaluate the hydration of human skin. *J. Applied Cosmetology*, **15**, 95–102, 1997

Appendix A

Experimental results

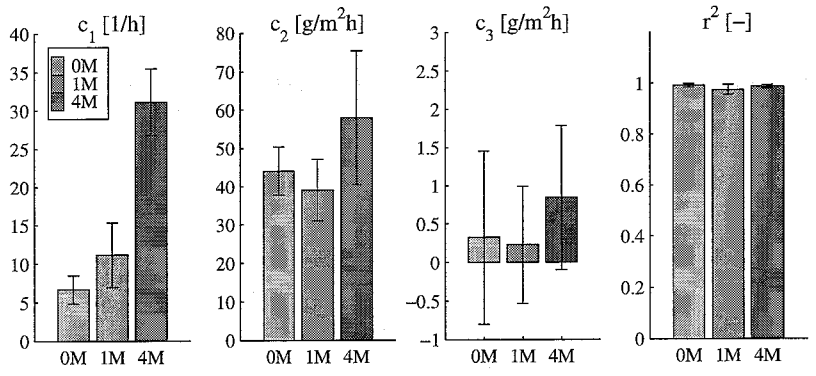

Figure A.1: Mean values (solid bars) and standard deviations (vertical lines) of the TEWL fit coefficients, as listed in table 3.1. Note a y-axis scaling of 10:20:1, from plot c_1 to c_3.

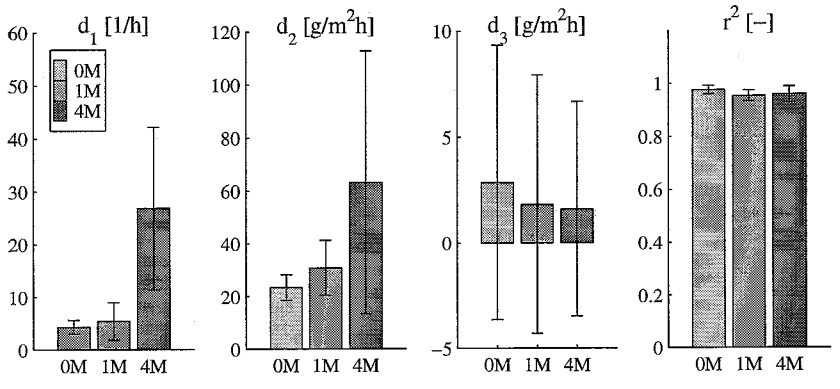

Figure A.2: Mean values (solid bars) and standard deviations (vertical lines) of the capacitance fit coefficients, as listed in table 3.3. Note a y-axis scaling of 4:8:1, from plot d_1 to d_3.

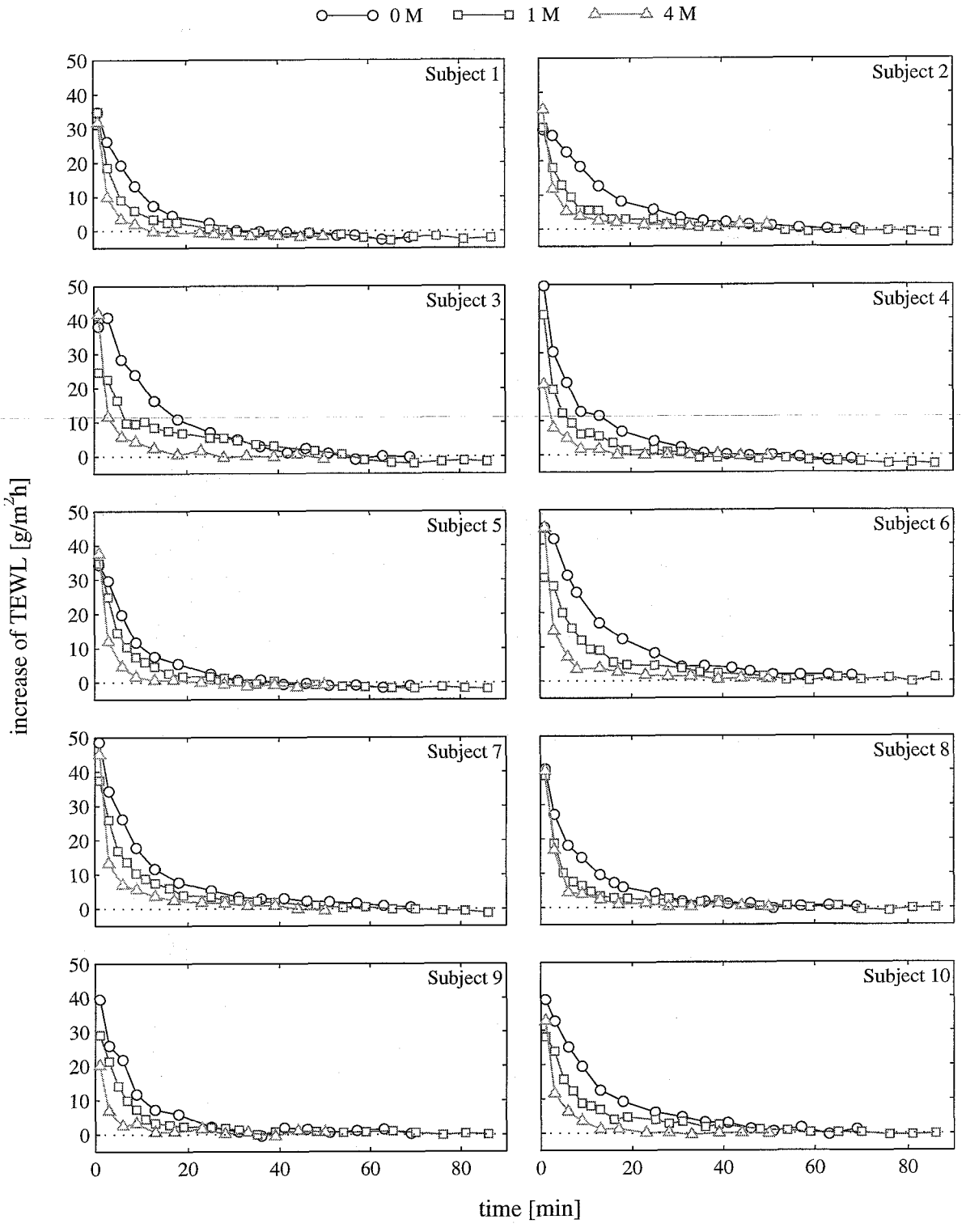

Figure A.3: Measured increase of TEWL after one hour application with distilled water (circles in black), 1 M (squares in dark gray), and 4 M NaCl solution (triangles in light gray) shown per subject.

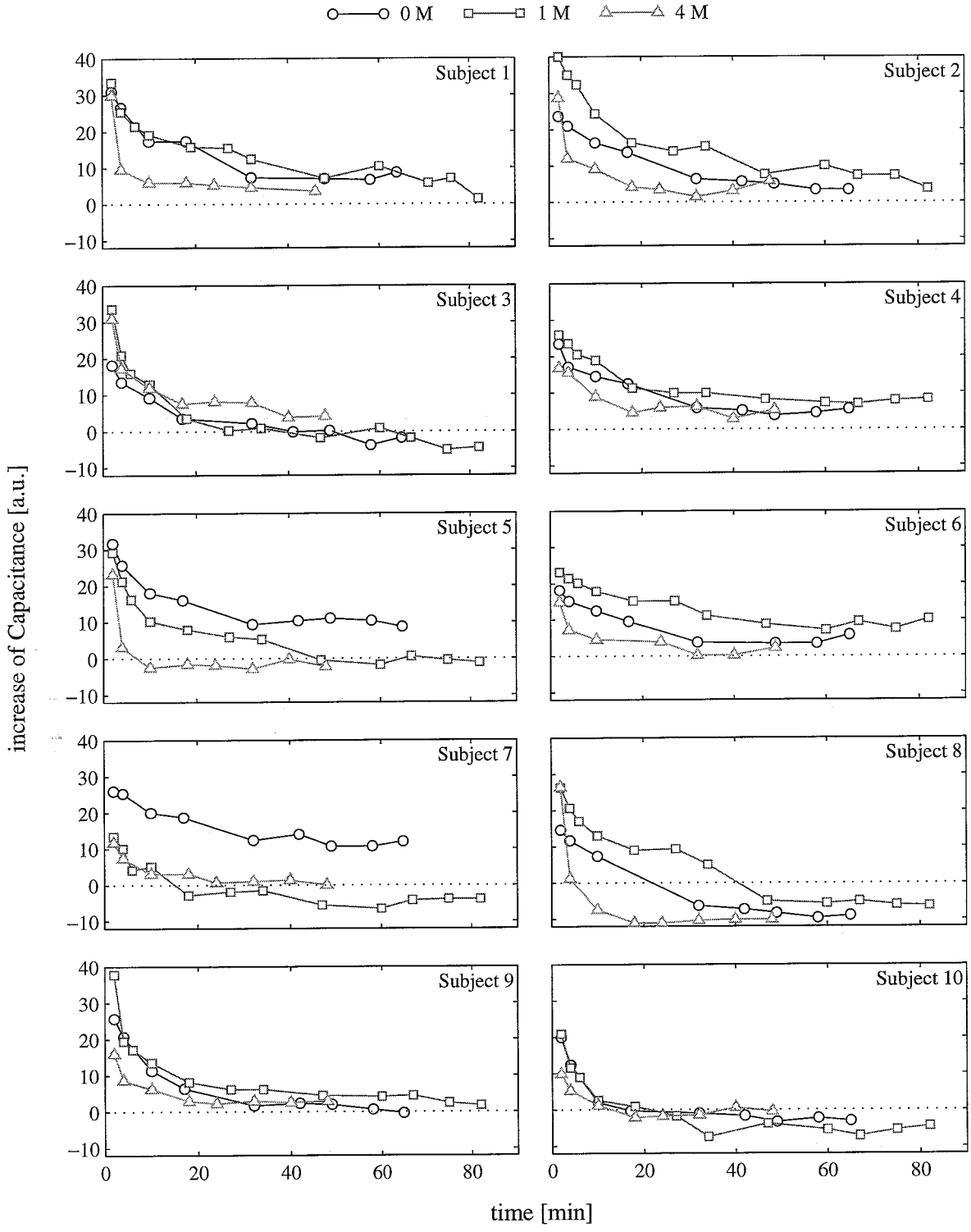

Figure A.4: Measured increase of electrical Capacitance after one hour application with distilled water (circles in black), 1 M (squares in dark gray), and 4 M NaCl solution (triangles in light gray), shown per subject.